

Graduate Thesis for Master of Science Diploma  
Physics and Engineering Physics  
Chalmers University of Technology

Performed at  
Volvo Technology Corporation



**CHALMERS**

# **SOFC Modeling in Femlab**

ANDERS NORDELÖF  
CHRISTOFER SALSING

Supervisor: Per Rutquist  
Volvo Technology Corporation

Examiner: Professor Bengt-Erik Mellander  
Physics and Engineering Physics  
Chalmers University of Technology

Göteborg, 2003



## Abstract

This report describes a graduate thesis project for the Master of Science diploma from the Engineering Physics program at Chalmers University of Technology. It has been performed at Volvo Technology Corporation with the primary aim to model a given Solid Oxide Fuel Cell design, the Rutquist cell, in Femlab. The model is intended to provide information on current-voltage characteristics, power development and the temperature profile, both during startup and operation. The secondary purpose was to evaluate the suitability of Femlab for this kind of task.

The project was initiated with a bibliographic research, which gave several theories and parameters useful for modeling the different processes in the SOFC design. These models were then implemented in Femlab. Two separate modes were created where the startup and the operation of the cell respectively, were simulated. The cell was assumed to be a part of a larger system and receive hot gases from a fuel reformer. The heating in the startup process was achieved by letting warm gas, 1073 K, enter the electrodes via the gas channels. The chemical reactions were assumed to begin when all parts of the structure had reached 1023 K. The calculations showed that the heating to this temperature takes about one minute, and that most of the heat exchange takes place in the electrodes. The resulting temperature profiles from the operation mode model demonstrate that the temperature is in the same range as other SOFC structures and that the design is very compact. The dimensions of a cubic stack developing 10 kW at maximum power would be less than one cubic decimeter.

The computational software Femlab has advantages, but also several shortcomings. Among the advantages are the flexibility in the module based system and the short learning period needed for solving simple problems. The weaknesses include the necessity of good knowledge of numerical solution methods, since many settings have to be adjusted when the models become more complex; especially the error report system is poor and occasionally even missing.

The report also presents the theory of the physical and chemical processes ceramic fuel cells. Suggestions for improvements and the effects of the delimitations and approximations used in the modeling work are discussed. Finally, recommendations for future work are put forward.



## Sammanfattning

Den här rapporten beskriver ett examensarbete utfört på Volvo Technology Corporation för civilingenjörsexamen vid Teknisk Fysik på Chalmers. Projektets syfte var att skapa ett analysverktyg för studier av fastoxidbränsleceller och analysera en given designidé, Rutquistcellen, med avseende på ström-spänningskaraktistik och effekt-utveckling samt temperaturfördelningen vid uppvärmning och drift. Modellen implementerades i beräkningsprogramvaran Femlab, vars lämplighet för denna typ av projekt samtidigt utvärderades.

Projektet inleddes med en litteraturstudie som ledde fram till ett antal teoretiska modeller och parametervärden som kunde användas för att beskriva de olika processerna i bränslecellen. Detta implementerades i Femlab i form av en tvådelad modell; uppvärmningen och driftsläget simulerades separat. Cellen antogs vara en del av ett system och föregås av en bränslereformator som lämnade ifrån sig en varm gasblandning till SOFC-strukturen. Uppvärmningen sker sedan genom att varm gas, 1073 K, från reformatorn blåses in i cellen och sprider sig via gaskanalerna till elektroderna. De kemiska reaktionerna antogs sätta igång när alla delar av strukturen nått 1023 K. Beräkningarna visade på att uppvärmningen till denna temperatur tar ungefär en minut och att det mesta av värmeutbytet sker i elektroderna. Resultaten, i form av temperaturprofiler, från beräkningarna på driftsläget visade att materialets temperatur är i samma storleksordning som andra typer av SOFC-strukturer. Dessutom är designen mycket kompakt då en kubisk stack som genererar 10 kW är mindre än en kubikdecimeter.

Beräkningsverktyget Femlab visade sig ha många fördelar men samtidigt också stora brister. Till de största fördelarna hör flexibiliteten hos det moduluppbyggda systemet för ”multifysik” samt den korta inlärningstiden för enklare problem. På minussidan finns kravet på goda kunskaper om numeriska lösningsmetoder då många inställningar måste göras av användaren när modellerna blir mer komplexa. Detta särskilt då felrapporteringsystemet är undermåligt och ibland obefintligt.

I rapporten presenteras även den underliggande teorin för de fysikaliska och kemiska processerna i en fastoxidbränslecell. Förslag på förbättringar och effekter av de begränsningar och approximationer som använts diskuteras. Slutligen ges rekommendationer för framtida arbete.



## Preface

We have found it very interesting to work with this SOFC modeling project. A topic has included both a touch of the scientific research front, and implementation of fundamental physical relations into computational software. Working with research of this kind was a new experience for both of us, and it offered tough challenges as well as rewarding moments.

This thesis project was undertaken with great enthusiasm and curiosity, but sometimes, when not even the strongest determination was enough, it was good to know whom to turn to. In this context we would like to present our most deeply felt gratitude towards the persons around us: Our fellow graduate thesis compatriots for their good humor, the interesting discussions and the social happenings. The Volvo Technology Corporation crew for the help, badminton matches and coffee breaks. Ingvar Albinsson at Physics and Engineering Physics for his time and helpful answers. Filip Edström and Anders Karlsson for critical comments. Anna Wallén for love, support and delicious pastries.

However, the persons we would like to thank with the most warmth are our supervisor at Volvo Technology Corporation, Per Rutquist and our examiner Professor Bengt-Erik Mellander at Physics and Engineering Physics. For their kind assistance, commitment and for believing in us.

Thank you

Anders & Christofer  
Göteborg, March 2003





# Table of Contents

<b>1 INTRODUCTION</b> .....	<b>1</b>
1.1 Background.....	1
1.2 Purpose .....	1
1.3 Research Questions.....	2
1.4 Method.....	2
1.4.1 <i>Theory</i> .....	2
1.4.2 <i>Implementation</i> .....	2
1.5 Disposition .....	3
1.6 Delimitations .....	3
<b>2 THEORY</b> .....	<b>5</b>
2.1 Basics of Ceramic Materials for SOFC .....	5
2.1.1 <i>Requirements</i> .....	5
2.1.2 <i>Standard Materials</i> .....	5
2.2 Mass Transfer in Gas Channels and Electrodes.....	6
2.2.1 <i>Flow types</i> .....	6
2.2.2 <i>General Aspects of Diffusion</i> .....	7
2.2.3 <i>Pressure Driven Diffusion</i> .....	7
2.2.4 <i>Maxwell-Stefan Binary Diffusion</i> .....	8
2.2.5 <i>The Dusty Gas Model</i> .....	9
2.3 Heat Transfer .....	11
2.3.1 <i>Thermal Conduction</i> .....	11
2.3.2 <i>Thermal Convection</i> .....	12
2.3.3 <i>Conduction and Convection</i> .....	12
2.3.4 <i>Boundary Film</i> .....	13
2.3.5 <i>Derivation of the Film Coefficient</i> .....	13
2.3.6 <i>The Nusselt Number</i> .....	14
2.4 Principles of Operation .....	15
2.4.1 <i>Chemical Reactions</i> .....	15
2.4.2 <i>Reaction Rate Limitations</i> .....	16
2.4.3 <i>The Nernst Potential</i> .....	16
2.4.4 <i>Cell Overpotential</i> .....	18
2.4.5 <i>Power Generation and Dissipation</i> .....	20
2.4.6 <i>Transformation of the Gas Compositions by Chemical Reactions</i> .....	21
2.4.7 <i>Heat Production from Chemical Reactions</i> .....	22
2.5 Electric Conduction in Ceramics .....	23
2.5.1 <i>YSZ</i> .....	24

2.5.2	<i>LaMnO<sub>3</sub></i> .....	25
2.5.3	<i>Mathematical Description</i> .....	25
<b>3</b>	<b>FEMLAB</b> .....	<b>27</b>
3.1	The Software .....	27
3.1.1	<i>Introduction to Femlab</i> .....	27
3.1.2	<i>The Femlab Module System</i> .....	27
3.2	Work Procedure .....	28
3.2.1	<i>The Graphical User Interface</i> .....	28
3.2.2	<i>Methodology</i> .....	28
3.3	The SOFC Model .....	29
3.3.1	<i>Implementing the Unit Cell</i> .....	29
3.3.2	<i>Implementing the Multiphysics</i> .....	29
<b>4</b>	<b>SOFC MODEL</b> .....	<b>31</b>
4.1	Modeling the Structure and Basic Conditions .....	31
4.1.1	<i>The Fuel Processor</i> .....	31
4.1.2	<i>The Original Structure and the Unit Cell</i> .....	32
4.1.3	<i>Material Parameters</i> .....	34
4.1.4	<i>Gas Parameters</i> .....	34
4.2	Bringing the Structure to the Temperature of Operation .....	35
4.2.1	<i>Heat Transfer Modes</i> .....	35
4.2.2	<i>Heat Convection from the Gas Channels</i> .....	36
4.2.3	<i>Gas Diffusion in the Electrodes</i> .....	37
4.3	Implementing Active Mode .....	37
4.3.1	<i>General Assumptions</i> .....	37
4.3.2	<i>Electric Conduction Modes</i> .....	38
4.3.3	<i>Stack Size and Power Generation</i> .....	40
4.3.4	<i>Ohmic Heat</i> .....	42
4.3.5	<i>Approaches to Model the Consumption of Reactants</i> .....	42
4.3.6	<i>Chemical Reaction Heat Generation</i> .....	44
<b>5</b>	<b>RESULTS</b> .....	<b>45</b>
5.1	Heating Mode .....	45
5.1.1	<i>Temperature profile</i> .....	46
5.1.2	<i>Pressure and velocity</i> .....	46
5.2	Active Mode .....	48
5.2.1	<i>Electric Characteristics</i> .....	48
5.2.2	<i>Temperature profile</i> .....	51
<b>6</b>	<b>DISCUSSION</b> .....	<b>53</b>
6.1	General overview .....	53
6.1.1	<i>The scope of the thesis</i> .....	53

6.1.2 <i>Delimitations and approximations</i> .....	53
6.2 Features in the model and its results .....	54
6.2.1 <i>Tabulated data</i> .....	54
6.2.2 <i>Gas composition and diffusion</i> .....	54
6.2.3 <i>The Rutquist cell</i> .....	55
6.3 Femlab.....	56
<b>7 CONCLUSIONS.....</b>	<b>57</b>
<b>8 FUTURE WORK.....</b>	<b>59</b>
<b>REFERENCES .....</b>	<b>61</b>
Cited Material .....	61
General Sources .....	63
<b>GLOSSARY .....</b>	<b>65</b>
<b>APPENDIX A: MATERIAL PARAMETERS.....</b>	<b>A-1</b>
<b>APPENDIX B: STANDARD STATE EMF POLYNOMIAL CURVE FITS .....</b>	<b>A-3</b>
<b>APPENDIX C: LOG FUNCTION POLYNOMIAL CURVE FIT .....</b>	<b>A-5</b>



# 1 Introduction

This diploma thesis describes the development of a high temperature fuel cell model made in *Femlab*, a computer software that uses the finite element method to numerically solve differential equations. In this introductory chapter the objectives for the project are presented together with the choices made regarding the method used, the disposition of the report and the delimitations for the project.

## 1.1 Background

The fuel cell is an invention from the first half of the nineteenth century that was brushed off and updated during the exploration of space in the 1960's. An increased demand for energy combined with progress in material research, led the fuel cell research and development into a period of high activity that has taken the technology to the brink of commercialization. This description applies to most types of fuel cells including high temperature cells, although other types are more common in the fuel cell applications of today. [1]

The name Solid Oxide Fuel Cell, abbreviated *SOFC*, was given to the cell type because its *electrolyte* is a solid oxide, a type of ceramic material. It differs from other fuel cell types in some major aspects. The electrolyte conducts oxygen ions instead of protons or positive ions. It contains no precious metals such as platinum or palladium. The fact that SOFC operates at a high temperature makes it possible to feed it with several different fuels. Thus, it is not limited to the use of hydrogen as some other types are. However, if these differences can be seen as advantages, there is also one major drawback: the production cost today is very high.

Nevertheless, there is a growing interest for the SOFC technology. An increased focus on the environmental consequences of energy conversion has created a motivation to improve fuel efficiency as well as reduce engine noise and emissions in the vehicle industry. In heavy vehicles, such as diesel driven trucks, an SOFC *stack* could be used to supply auxiliary power for overnight use of air-conditioning and on-board electronics or to complement the propulsion power during driving sessions, for example by refrigerating the cargo. The SOFC is well suited for *APU*<sup>1</sup> use with today's conventional fuel. [2]

At Volvo Technology Corporation, coworker Per Rutquist had introduced an SOFC design idea that differs from ordinary SOFC stack solutions. The company was therefore interested in building an analyzing tool and to conduct a thorough investigation of the basic properties displayed by the new design. Volvo Technology Corporation also suggested that the work could be performed in a *Matlab* based program called Femlab, marketed as a powerful instrument for computational modeling.

## 1.2 Purpose

This diploma thesis has been performed with several purposes. Primarily, the aim has been to model the given SOFC structure in Femlab using first principle equations and thereby create a tool for the analysis of ceramic fuel cells. The model was intended to

---

<sup>1</sup> APU stands for Auxiliary Power Unit.

provide the current-voltage characteristics during operation and present the dimensions of a stack delivering 10 kW at maximum power. Furthermore, the most desired feature sought was the temperature profile in the structure, calculated with consideration to all essential parameters, both during startup and operation. The secondary purpose of the thesis has been to evaluate Femlab's suitability for this type of work and to give guidelines and advice to future users.

### 1.3 Research Questions

The purpose presented above was reformulated into four research questions:

- Can a simple model of the given structure be created from first principle equations and serve as an analyzing tool?
- What current-voltage characteristics does the given structure display and how large is a 10 kW stack?
- How does the temperature distribution develop during the heating phase and what is the result at steady-state operation?
- Is Femlab a suitable tool for this type of modeling?

### 1.4 Method

The project work can be seen as divided into two phases starting with the theoretical part, where the underlying models and theories were studied, followed by the practical part where the preceding results were implemented in Femlab. This is however not to be regarded as strict chronological division since many times, when working with Femlab, it was necessary to go back to the textbooks and theories.

#### 1.4.1 Theory

Initially the main concern was to perform a literature study, scanning all available publications for information on earlier work in the area. While doing this survey, another aim was to find relevant material parameters for the model. However, there was not much published data to be found, neither on the Internet nor in the library. This made it necessary to look further into theories and models describing first principal relations and physical phenomena. Additionally, the scope of the first project phase was to create a good understanding of general SOFC theory.

#### 1.4.2 Implementation

Having established the theoretical framework, the next step was to implement the mathematical models in Femlab and connect them to the model geometry. Using different so called *modes*, the physical phenomena could be modeled separately. The mathematical formulations, derived by the producers of the software, often had to be adapted which also implied that new physical correlations and constants had to be found in literature in order to use the built-in functions. The modes were then incorporated into a complete model by linking the modes and variables to each other. Much effort had to

be put on making sure that the coupled systems generated equations that Femlab actually was able to solve, and doing it in a reasonable time.

## **1.5 Disposition**

The report has been written to ensure the best possible comprehensibility, and effort has been put on creating an outline that will guide the reader through the text in the most logical way. This document consists of four basic parts. Starting off there is the introduction which describes the purpose of the thesis project, the delimitations made, the methods used and the context in which the project was undertaken as well as Volvo Technology Corporation's interest in the project.

Following the introduction there is the theory part, which gives a detailed picture of the different materials modeled and the physical phenomena incorporated. This part examines the characteristics of mass and heat transfer together with the electrical conduction and the underlying chemical reactions in the SOFC. The third and fourth sections consider the design and structure of Femlab and the implementation of the theoretical models. This part of the report is more pragmatic and handles questions arising on how to deal with practical considerations, such as geometry design and approximations. It also describes the two parts of the model, namely the "*Heating Mode*" and the "*Active Mode*".

Finally the report is rounded off by presenting achieved results, discussing these and introducing the drawn conclusions, followed by suggestions and recommendations for future work. Supplementary information on the work along with references can be found on the pages after that section.

## **1.6 Delimitations**

In order to complete the project in the time available it was necessary to reduce the original scope. Considering the given facilities and resources certain delimitations were made. The most important one was to reduce the model space into two dimensions. The studied unit cell was also considered to be in the center of a large stack, thus making it possible to ignore boundary effects. Furthermore, applying approximations and simplified assumptions to the different model parts reduced the model complexity.

The gas channels only appear in the model as boundary conditions and the mass transfer models do not consider binary diffusion. Additionally, the consumption of the reactants at the electrolyte interface was described by a simplified model and the interface itself was considered to be one-dimensional. These assumptions were considered carefully and, from the results, not found to reduce the usefulness and predictability power of the model. Finally the model was divided into separate parts to make it easier to work with. The result was, as mentioned above, one model for the Heating Mode and another for the Active Mode.

In Heating Mode the model describes the pre-heating where hot gas is pressed through the structure in order to make the material reach the wanted working conditions. The structure was assumed to initiate from room temperature. In this mode the assumption is that no chemical reactions take place. The Active Mode model was developed in order to give the electrical characteristics and temperature distribution during operation. It also encompasses some delimitations; the mode is assumed to be

stationary, i.e. it does not change over time, and the consumption of the reactants had to be substantially simplified.



## 2 Theory

This chapter presents all essential theory that was used in the modeling work. It includes the fundamentals of ceramic materials, mass and heat transfer along with the principles of operation and electric conduction in ceramics.

### 2.1 Basics of Ceramic Materials for SOFC

In order to generate electrical energy the electrolyte of a fuel cell must ionically conduct charge carriers through the electrode. In an SOFC three different types of ions are possible: oxygen ions, hydrogen ions or hydroxide ions. Nevertheless, to current date almost all development work has been focused on ceramic oxygen-ion conducting electrolytes such as *zirconia*. In this section the basic requirements on the SOFC materials are presented together with the most common choices in today's technology. However, the electric properties for the different materials are treated in a separate section at the end of this chapter.

#### 2.1.1 Requirements

An SOFC electrolyte must be a good oxide ion conductor over a large range of oxygen partial pressures. At the same time it must have very low *porosity* and *permeability* in order not to leak gas from one electrode to the other. This is especially important since the electrolytes in general are made very thin because of the relative difference in conductivity compared with the electrodes in order to minimize internal resistive losses.

In the electrodes, gas has to be transported a considerable distance by means of diffusion. Therefore, the materials must have significant porosity to allow gas transport to the reaction sites. At the same time, considerations have to be taken both to the electrical properties and the mechanical strength. Values between 10 to 50 percent are possible [3]. The lower limit is set by mass transport phenomenon and the upper limit is based on requirements on the strength of the material. The electrical conductivities for the electrode materials are in general good.

In most SOFC designs it is also necessary to have an interconnecting material that preferably has good conductivity along with low porosity and permeability. For all materials it is important that they do not interact chemically with each other and that they remain stable both in an oxidizing and reducing environment. Furthermore, it is crucial that the used materials have about the same heat expansion coefficient. A bad match will result in internal tensions and crack growth. [3]

#### 2.1.2 Standard Materials

The customary choice for the electrolyte in SOFC technology today is *yttria-stabilized zirconia* (YSZ). It does not have the highest conductivity among the different types of stabilized zirconia, but it is the most easily accessible and has the lowest cost. It meets all the requirements stated above but the SOFC has to be operated at 800-1000°C<sup>2</sup> in order to reach acceptable electric conduction.

---

<sup>2</sup> In the SOFC model, all temperatures are specified in Kelvin (K), whereas some of the literature on ceramic materials uses Celsius (°C).

For the anode a *cermet* of YSZ and nickel (Ni/YSZ) is most commonly used. The nickel gives the structure its porosity and good electrical conductivity while the YSZ provides stability and compatibility with the other components. Nickel is used because of its low cost in comparison with other metals that gives the same result such as platinum or palladium.

The standard material for the cathode is lanthanum manganite ( $\text{LaMnO}_3$ ). It has a high electrical conductivity and several of its parameters, e.g. the porosity, can be tailored to match those demanded in the structure. However, it has a tendency to interact with the surrounding materials and precautions must be taken during the fabrication in order to minimize this. It is often doped with strontium to optimize its performance.

The interconnect material that is most common is lanthanum chromite  $\text{LaCrO}_3$ . It has good stability in the environment and good compatibility with the other components. Similar to  $\text{LaMnO}_3$  it is doped to get better conductivity. [3]

## 2.2 Mass Transfer in Gas Channels and Electrodes

Transport phenomena are of great importance for the functioning of a fuel cell. To be able to create a realistic model it is essential to know how gases are transported through the structure. The concentration and pressure of the gases at a specific point in the material define the basic input for the description the heat transfer and the chemical reactions. The main interest lies in modeling the flow in the open gas channels and the diffusion of gases in the porous electrodes.

### 2.2.1 Flow types

The terms *pipe flow* and *channel flow* are used for viscous incompressible flow through a tube of uniform circular cross-section. In one end the fluid<sup>3</sup> is supplied at a constant pressure that is higher than the constant pressure at the other end. The fluid is pushed through the pipe from the high-pressure end to the low. Gravitational force is normally neglected because of its low impact in comparison with the forces related to the pressure differences. Pipe flow refers to the three-dimensional tube whereas channel flow describes the two dimensional counterpart where the flow is supposed to occur between two parallel walls.

In fluid dynamics there is a distinction between two main types of flow, *laminar* and *turbulent*. Channel flow is regarded as laminar when the velocity profile of the fluid is parabolic as in Figure 2–1. The shape can be explained with continuum mechanisms between assumed fluid particles that also have a no-slip condition at the wall. The speed at a certain position is always the same and each fluid particle travels along a simple well-defined path. The concept of fluid particles originates from the continuum hypothesis which introduces fluid particles that are small enough to be regarded as points in the flow but still large enough to contain a considerable number of molecules. Laminar channel flow is often also assumed to be *fully developed* which means that the velocity profile does not vary along the line of the flow. When the flow becomes turbulent all regular paths are distorted. Fluid particles that start at the same position travels along different paths and the irregularities change continuously. [4]

---

<sup>3</sup> A fluid is defined as a substance that deforms continuously when it is exposed to shear stress. Both liquids and gases are fluids. [4]

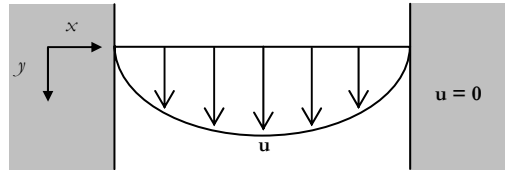


**Figure 2-1:** *Velocity profile for laminar channel flow* [4].

There are several different variables that determine the pipe and channel flow: the geometric dimensions, the rate of flow and the physical properties of the fluid. The parameters that are required for a description that is valid for most situations are the pipe diameter  $d$ , the average speed  $u_{av}$ , the fluid density  $\rho$  and the viscosity  $\eta$ . Together these parameters can be combined into a dimensionless parameter known as the *Reynolds number*.

$$\text{Re} = \frac{\rho u_{av} d}{\eta} \quad (2-1)$$

It has been found experimentally for pipe flow that the flow is always laminar when the Reynolds number is below 2300. This value is therefore regarded as a critical number and when it is surpassed transition to turbulent flow sometimes occurs. However, laminar flow has been observed for Reynolds numbers as high as 40000. [5]

### 2.2.2 General Aspects of Diffusion

When a gas mixture contains two or more molecular species, whose relative concentration vary from point to point, a process follows which tends to minimize the concentration differences. This macroscopic mass transfer is by definition called *molecular diffusion* and the net molecular flow of each molecular species will be in the direction of the negative concentration gradient.

In a porous media this mass transfer can take place in three different ways. First there is *bulk diffusion*, also known as *Fick diffusion*, which is the predominant mechanism in a material with relatively large pores and a dense gas mixture. Second there is *Knudsen diffusion*, which describes the case when the mean free path of the diffusing molecules is much larger than the diameter of the pores and consequently molecule-wall collisions become important. Finally the diffusion can also occur through so called *surface diffusion* where adsorbed molecules are forced to move due to two-dimensional concentration gradients. This kind of diffusion becomes dominant for micropores and for strongly adsorbed species. [5, 6, 7]

### 2.2.3 Pressure Driven Diffusion

Porous materials can be described by different material parameters such as porosity and *tortuosity*. The porosity describes the fraction of void space in the material whereas the tortuosity links the actual path length to the nominal length of the porous media. In other words, a material where the diffusion paths are tortuous, the pores and channels are irregularly shaped and the flux is less than it would be in a material with pores of the same length and mean radius. The tortuosity will naturally affect the rate of diffusion in the

material and consequently also the *diffusion constant*. Considering only the bulk diffusion, the molar flux can be written with the Fick rate equation [5].

$$\mathbf{J} = -D_{\text{eff}} \nabla c \quad (2-2)$$

The diffusion constant is denoted as effective since it accounts for the porosity and tortuosity unlike the regular diffusion constant, denoted  $D_{AB}$  with the indices  $A$  and  $B$  indicating that the substance  $A$  is diffusing through substance  $B$ . The effective diffusion constant can be derived from the regular constant using the porosity  $\varepsilon$  and the tortuosity  $\tau$  [6, 7].

$$D_{\text{eff}} = \frac{D_{AB} \varepsilon}{\tau} \quad (2-3)$$

It can be noted that Fick's law postulates a linear dependence of the flux  $\mathbf{J}$  with respect to the molar average mixture velocity, which is given as the gradient of the concentration  $c$  for the diffusing specie. Sometimes it can be more convenient to formulate the model using pressure instead of concentration. The only difference is that the diffusion coefficient has to be transformed accordingly. A theory that describes pressure driven diffusion through a porous medium is Darcy's law. This law relates the velocity of the diffusing fluid  $\mathbf{u}$  to the permeability  $k$ , the viscosity  $\eta$  and the pressure  $p$ .

$$\mathbf{u} = \frac{k}{\eta} \nabla p \quad (2-4)$$

In order to compensate for the compressibility of the fluid, equation (2-4) can be used together with the continuum equation

$$\nabla \cdot (\rho \mathbf{u}) = 0 \quad (2-5)$$

with  $\rho$  denoting the density of the diffusing media. The combination yields

$$\nabla \cdot \left( -\rho \frac{k}{\eta} \nabla p \right) = 0 \quad (2-6)$$

This equation can then be used for studying homogenous compressible flow through a porous structure. [5, 6, 8]

## 2.2.4 Maxwell-Stefan Binary Diffusion

Fick's law only accounts for the interaction between the diffusing gas and the *solvent*. For a solution that contains several species a correct description must include the interaction between them. This type of *multicomponent diffusion* is described by the Maxwell-Stefan equations. The derivation starts from the joint diffusion of two species and the theory is therefore also referred to as *binary*. Using a generalized and extended formulation of the Fick rate equation, it yields

$$\mathbf{N}_1 = -cD_{12}\nabla\kappa_1 + \kappa_1(\mathbf{N}_1 + \mathbf{N}_2) \quad (2-7)$$

for the first of the two species, where  $\mathbf{N}_i$  stands for the molar flux for each species,  $\kappa_i$  for the molar fraction and  $D_{ij}$  is the Maxwell-Stefan *diffusivity* that is related to Fick's diffusion constant via a thermodynamic factor [5, 6]. For ideal liquid mixtures at low pressures this factor is one. The formulation of the equations can be done in several different ways. The same equation can be stated for the mass flux as well as molar flux, using mass fraction instead of the molar fraction. This also implies a switch from the concentration to the density, but the diffusion coefficient remains the same. However, if (2-7) is retained, the next step is to formulate the equation for  $n$  species, instead of only two.

$$\nabla\kappa_i = \sum_{j=1}^n \frac{\kappa_j\mathbf{N}_i + \kappa_i\mathbf{N}_j}{cD_{ij}}, \quad i = 1, 2, \dots, n \quad (2-8)$$

This is the multicomponent formulation of the Maxwell-Stefan equations and it can be seen that it includes binary diffusion constants. For the general case this diffusivity can be calculated from an empirical relation using the temperature and the pressure together with fixed, experimentally determined values for the incorporated gas. It includes the molar volume  $v_i$  and the molar mass  $M_i$  for each species along with a correlation constant  $K$  that is set to  $1.43 \times 10^{-7}$  and gives the diffusion constant in  $\text{m}^2/\text{s}$  [9].

$$D_{ij} = \frac{K}{\sqrt{2}} \cdot \frac{T^{1.75}}{p(v_i^{1/3} + v_j^{1/3})^2} \sqrt{\frac{1}{M_i} + \frac{1}{M_j}} \quad (2-9)$$

When there are external forces or gradients driving the diffusion system they also have to be taken into account. An external driving force also encompasses that linear momentum will be conserved. For the diffusion in a porous ceramic, where mechanical equilibrium is established much faster than thermodynamic equilibrium, this can be expressed as [6]

$$-\frac{1}{\rho}\nabla p + \frac{\rho_i}{\kappa_i} \sum_{k=1}^n c_k \mathbf{F}_k = 0, \quad i = 1, 2, \dots, n \quad (2-10)$$

$\mathbf{F}_k$  represents the force acting on each mole of species  $k$ . If this expression is combined with (2-8) it yields the Maxwell-Stefan equations for multiple components with external driving forces [6].

$$-\nabla\kappa_i - \frac{(\kappa_i - \omega)_i}{p'} \nabla p + \frac{1}{p} \left( c_i \mathbf{F}_i - \omega_i \sum_{i=1}^n c_i \mathbf{F}_i \right) = \sum_{j=1}^n \frac{\kappa_j \mathbf{N}_i - \kappa_i \mathbf{N}_j}{cD_{ij}}, \quad i = 1, 2, \dots, n \quad (2-11)$$

### 2.2.5 The Dusty Gas Model

Assuming that the most significant contribution to the mass transfer is due to a combination Fick and Knudsen diffusion, the most convenient approach to model this phenomenon is the *Dusty Gas Model*, an application of the Maxwell-Stefan equations. The

basic assumption is that the pore wall can be modeled as a structure of giant molecules, or “dust” bubbles that are uniformly distributed in space. These are not considered to take part in the diffusion like the ordinary species. Instead they are held motionless in space. For an  $(n+1)$ -component mixture, equation (2–11) is rewritten to

$$-\nabla \kappa_i' - \frac{(\kappa_i' - \omega_i)'}{p'} \nabla p' + \frac{1}{p'} \left( c_i \mathbf{F}_i - \omega_i' \sum_{i=1}^{n+1} c_i \mathbf{F}_i \right) = \sum_{j=1}^{n+1} \frac{\kappa_j' \mathbf{N}_i - \kappa_i' \mathbf{N}_j}{c D_{ij}'}, \quad i = 1, \dots, n+1 \quad (2-12)$$

The primed variables refer to the pseudo-mixture that includes both the diffusing gas species and the dust molecules, whereas the unprimed ones refer only to the gas and have physical meaning.

To obtain valid equations for the Dusty Gas Model the following assumptions have to be made:

- the dust concentration  $c_M$  is spatially uniform.
- the dust is motionless, so that  $\mathbf{N}_{n+1} = 0$ .
- the molar mass of the dust particles approaches infinity,  $M_{n+1} \rightarrow \infty$ .

This means that the dust molecules must be constrained by external forces  $\mathbf{F}_{n+1}$ . The dust is clamped in place and the molecules are prevented from moving in response to gas pressure gradients.

$$\nabla p = c_{n+1} \mathbf{F}_{n+1} \quad (2-13)$$

It is assumed that there are no external body forces acting on the diffusing species. Having made these assumptions it is possible to write the first  $n$  equations as

$$-\nabla \kappa_i' - \frac{(\kappa_i' - \omega_i)'}{p'} \nabla p' - \frac{\omega_i'}{p'} c_{n+1} \mathbf{F}_{n+1} = \sum_{j=1}^n \frac{\kappa_j' \mathbf{N}_i - \kappa_i' \mathbf{N}_j}{c' D_{ij}'} + \frac{\kappa_{n+1}' \mathbf{N}_i}{c' D_{i,n+1}'}, \quad i = 1, 2, \dots, n \quad (2-14)$$

Transforming the primed variables from the pseudo-mixture to the unprimed gives us the relevant variables for the gas.

$$D_{ij}^e = \frac{c' D_{ij}'}{c} \quad (2-15)$$

$$D_{iM}^e = \frac{D_{i,n+1}'}{\kappa_{n+1}'} \quad (2-16)$$

The result obtained is [6]

$$-\frac{1}{RT} \nabla p_i = \sum_{j=1}^n \frac{\kappa_j' \mathbf{N}_i - \kappa_i' \mathbf{N}_j}{D_{ij}^e} + \frac{\mathbf{N}_i}{D_{iM}^e}, \quad i = 1, 2, \dots, n \quad (2-17)$$

The  $D_{ij}^e$  represents the effective binary pair diffusion coefficients in the porous medium, while  $D_{iM}^e$  is the effective Knudsen diffusion coefficients. The  $D_{ij}^e$  can be linked to the free space values by

$$D_{ij}^e = \frac{D_{ij} \varepsilon}{\tau} \quad (2-18)$$

where  $\varepsilon$  is the porosity, and  $\tau$  the tortuosity, as stated in 2.2.3. There are theoretical models for evaluating these parameters but they are however best determined by experiment. For a cylindrical pore the value for the tortuosity is unity. The free space binary diffusivities  $D_{ij}$  has already been presented in the previous section and the effective Knudsen diffusivities are

$$D_{iM}^e = (\varepsilon / \tau) \frac{d_p}{3} \sqrt{\frac{8RT}{\pi M_i}} \quad (2-19)$$

where  $d_p$  is the pore diameter and the square-root term represents the velocity of motion. The expression is given in m<sup>2</sup>/s. [6]

## 2.3 Heat Transfer

In a fuel cell model it is crucial to pay attention to heat transfer and heat exchange processes. Thermal energy transferred from the electrochemical reactions, ohmic losses and the incoming gas flow to the structure, can potentially cause heat concentrations and heat sinks. Heat gradients in space and in time generate tension and mechanical stresses. It is therefore important to control the distribution and transfer of heat in the structure to prevent crack growth and material deterioration.

### 2.3.1 Thermal Conduction

The most significant part of the energy transfer in solids occurs as conduction. It can be accomplished in two ways, molecular interaction or free electron movement. In the first mechanism, which occurs in all materials, energy is imparted from molecules with high energy to neighboring molecules with lower energy. Free electron transfer occurs primarily in metallic solids due to the high concentration of free electrons and it is the explanation to why pure metals are such good heat conductors. In conduction the heat flux is proportional to the temperature gradient, which is described by the Fourier rate equation,

$$\frac{q}{A} = -k \nabla T \quad (2-20)$$

where  $q$  is the rate of heat transfer and  $A$  the area normal to the direction of the heat flow,  $k$  the thermal conductivity and  $\nabla T$  the temperature gradient. The value for  $k$  varies along with the material. The general equation that describes how the temperature changes

in time and space due to thermal conduction includes these terms. It is commonly referred to as the time-dependent heat equation.

$$\rho C_p \frac{\partial T}{\partial t} - \nabla \cdot (k \nabla T) = Q \quad (2-21)$$

$Q$  represents a volume heat source, e.g. heat generated by ohmic resistance or heat exchanged between the solid and a gas,  $\rho$  is the density and  $C_p$  the specific heat capacity. [5, 8]

### 2.3.2 Thermal Convection

Energy exchange between a surface and an adjacent fluid is associated with convection, which is either *free* or *forced*. It presumes a temperature difference between the fluid and the surface. Free convection means that the temperature difference causes density differences in the fluid that result in circulation of the fluid. Forced convection refers to a situation where the fluid is made to flow past the surface by an external agent, for example a fan. The rate equation for convection was originally set up by Newton. It is

$$\frac{q}{A} = b \Delta T \quad (2-22)$$

where  $b$  is the heat transfer coefficient,  $\Delta T$  the temperature difference between the fluid and the surface, and as above,  $q$  represent the rate of heat transfer and  $A$  the area normal to the direction of the heat flow. [5]

### 2.3.3 Conduction and Convection

A gas that is diffusing through a porous material exchanges thermal energy with its surroundings and the resulting process aims at minimizing the temperature differences. The gas diffuses with a certain speed through the structure and delivers or removes energy. To fully describe this process the gas velocity has to be known along with how the energy is transferred between the gas and material. This heat transfer with the surrounding structure and how the heat diffuses within the gas can be modeled with a combined conduction and convection heat equation, i.e. by adding conductive flux term to equation (2-21),

$$\rho C_p \frac{\partial T_g}{\partial t} + \nabla \cdot (-k \nabla T_g + \rho C_p T_g \mathbf{u}) = Q \quad (2-23)$$

with

$$Q = H(T - T_g) \quad (2-24)$$

The  $\mathbf{u}$  is the gas velocity,  $Q$  is the term that governs the exchange of thermal energy between gas and structure,  $\rho$  is the density and  $C_p$  the specific heat capacity, as in the previous section. Here  $Q$  is assumed to stand for some type of convection relation. In the



case of a porous material, the constant  $H$  can be evaluated by considering a forced convection equivalent, and then compensating for the porosity of the solid material.

### 2.3.4 Boundary Film

In a flow past a surface there is always a layer close to the surface where the profile is laminar regardless if the flow is laminar or turbulent in the main flow. Also, the fluid particles next to the surface are always at rest. This means that heat transfer involve conduction through a fluid layer or *film* close to the surface, which acts as the controlling resistance to convective heat transfer. For this reason the coefficient  $h$  sometimes is referred to as the *film coefficient* at the interface between a flowing fluid and a solid body. It is calculated using the fluid and flow properties in the film. In this evaluation it is customary to use the film temperature, calculated as

$$T_f = \frac{T_{wall} + T_{channel}}{2} \quad (2-25)$$

i.e. the arithmetic mean between the wall and the main flow of the fluid [5].

### 2.3.5 Derivation of the Film Coefficient

The heat transfer rate at the interface between the wall and the fluid can be written in terms of convection, as

$$q_x = hA_{wall}\Delta T_x \quad (2-26)$$

However, as stated in the section above, the heat transfer rate can also be formulated at the film surface as

$$q_x = -kA_{channel}\theta \left. \frac{\partial T}{\partial x} \right|_{surface} \quad (2-27)$$

where  $\theta$  represents the porosity of the gas channel [10]. Since these two terms have to be equal, and the fact that the wall area and the channel area multiplied with the porosity must be the same, yields

$$h\Delta T_x = -k \left. \frac{\partial T}{\partial x} \right|_{surface} \quad (2-28)$$

An approximation of the derivative at the surface gives

$$-\left. \frac{\partial T}{\partial x} \right|_{surface} \approx \frac{\Delta T_x}{\Delta x} = \frac{\Delta T_x}{d_f} \quad (2-29)$$

where  $d_f$  is the width of the boundary film and the negative sign on the right side has been included in the temperature difference term. Equation (2-28) can be rewritten to

$$b = -\frac{k}{\Delta T_x} \frac{\partial T}{\partial x} \Big|_{\text{surface}} \approx \frac{k}{\Delta T_x} \frac{\Delta T_x}{d_f} = \frac{k}{d_f} \quad (2-30)$$

Thus, if the width of the film and the thermal conductivity in the film are known, the heat transfer coefficient  $b$  at the interface between the fluid and the wall, i.e. the film coefficient, can be determined.

### 2.3.6 The Nusselt Number

The ratio of conductive thermal resistance to convective thermal resistance in a fluid is a dimensionless parameter referred to as the *Nusselt number*. The conductive thermal resistance is defined by

$$R_{\text{conduction}} = \frac{L}{kA} \quad (2-31)$$

where  $L$  is the length,  $A$  the cross-section of a given geometry, and  $k$  the thermal conductivity, as above [5]. The convective thermal resistance is defined in a similar way,

$$R_{\text{convection}} = \frac{1}{hA} \quad (2-32)$$

with  $L$  left out and  $k$  switched to the heat transfer coefficient  $h$  for the fluid. This gives the following result for the Nusselt number.

$$\text{Nu} = \frac{R_{\text{conduction}}}{R_{\text{convection}}} = \frac{hL}{k} \quad (2-33)$$

When heat is transferred from the flow to the wall in pipe or channel flow, the length  $L$  is equal to the tube diameter  $d$ . [5] Reformulation of (2-33) gives

$$h = \frac{k \cdot \text{Nu}}{d} \quad (2-34)$$

This supports the result in the previous section and a comparison of (2-30) with (2-34) makes it possible to identify the following expression.

$$d_f = \frac{d}{\text{Nu}} \quad (2-35)$$

The Nusselt number is commonly set to three as a first approximation for pipe flow [10, 11].

## 2.4 Principles of Operation

When the structure has reached its operating temperature, electric conduction through the electrolyte becomes possible and chemical reactions between the gases in the fuel and in the air begin. A brief description of the different types of electric conduction in the cell will be given further ahead in the report. Prior to that, this section explains the most essential parts in order to build an adequate model of the structure during operation. This includes the coupling between the chemical reactions and the electromotive force as well as *overpotential* and heat generation.

### 2.4.1 Chemical Reactions

The chemical reactions that constitute the driving force for the operation of an SOFC occur in the electrodes, mainly at the electrolyte borders. Oxygen from the air is reduced in the cathode and elements in the fuel are oxidized in the anode. These elements are hydrogen, carbon monoxide and methane. Hydrogen is oxidized most willingly of the three. The carbon monoxide and the methane can either be directly oxidized or react with water in the fuel gas and produce more hydrogen to uphold equilibrium. The degree of oxidation naturally also depends on the amount of each specific species present in the fuel. If a *reformer* generating mainly hydrogen and carbon monoxide, and only small quantities of methane, precedes the stack, the process can be approximated by direct oxidation of both hydrogen and carbon monoxide.

At the cathode oxygen molecules are split and react with electrons from the surrounding structure. This can be written as



The oxygen ions are then conducted through the electrolyte to the anode where they react with either hydrogen or carbon monoxide according to the following,



This gives the overall reactions in the fuel cell as



There is a difference in energy between the left and the right side in both reactions known as the *reaction enthalpy*,  $\Delta H$ . For both (2-39) and (2-40) the enthalpy is negative when the reaction goes to the right which means that energy is released. In reactions where the enthalpy is positive energy has to be absorbed in order to occur. For every reaction there is also a reaction rate that varies with the concentration of the involved species and a temperature dependent reaction coefficient. A comparison of the reaction rates makes it possible to decide the proportion each of the given reactions stands for when the fuel is consumed. However, all reaction rates at the electrode-electrolyte

interface can be assumed to be faster than the ion-diffusion through the electrolyte and that also includes the following balancing reaction that occurs.



At an operating temperature of 800°C<sup>4</sup> the equilibrium constant  $K$ , which is explained in the next section, is approximately equal to one [12]. This means that the production of water and carbon dioxide, together with the consumption of hydrogen and carbon monoxide, can be determined using the existing concentrations of the consumed species. [13]

### 2.4.2 Reaction Rate Limitations

Chemical reactions that depend on gas diffusion either for the supply of a reactant or to remove a reaction product can usually be placed into one of two categories. First, there are those processes that are controlled by the diffusion rate of the gas and where the chemical reaction is seen as a comparatively fast or as an instant process taking place at the reaction site. The total rate of the reaction is thus limited by the diffusion rate. The material supplied this way is immediately consumed at the reaction sites. These processes are called *diffusion limited reactions*.

In the other case, when the overall rate of the process is determined by the chemical reactions taking place at the reaction site, the process is a *reaction limited reaction*. The diffusion rate is in this case regarded as fast compared to the chemical reaction rate. It is therefore the chemical reaction rate that sets the upper limit for the overall reaction rate.

The chemical reaction rate is often slower than the diffusion rate at low temperatures and faster at higher temperatures. This is due to the fact that the activation energies for chemical reactions are usually larger than those for molecular diffusion. [7, 14]

### 2.4.3 The Nernst Potential

The energy from chemical reactions available to generate electric potential is commonly referred to as the change in free enthalpy, or *Gibb's free energy*,  $\Delta G$ . In order to balance the electrochemical reactions above, the Gibb's free energy must be compensated by enough energy to transfer the corresponding amount of electric charge between the different phases. If  $z$  is set to denote the number of charge equivalents needed for the formation of one mole of product this can be written as

$$zF \cdot \Delta V + \Delta G \leq 0$$

with  $F$  as Faraday's constant, which gives the charge of one mole electrons [1]. At equality the voltage introduced in the equation is the maximum potential difference that  $\Delta G$  can bring about and it is called the *electromotive force*, abbreviated as *EMF*,

---

<sup>4</sup> See note 2.

$$E_r = -\frac{\Delta G}{zF} \quad (2-42)$$

The electromotive force is also referred to as the *Nernst potential*, or the reversible thermodynamic voltage and it is therefore denoted  $E_r$ . Nernst was one of the most prominent figures in early chemical thermodynamics and he has given his name to the following equation.

$$E_r(T) = \frac{RT}{zF} (\ln K(T) - \ln \Phi(T)) \quad (2-43)$$

where  $\Phi$  is the reaction quotient,  $K$  the equilibrium constant and  $R$  the universal gas constant. The reaction quotient for an equation of the type



is, if the reactants are ideal gases, defined as

$$\Phi = \frac{[p_C]^c}{[p_A]^a [p_B]^b} \quad (2-45)$$

where  $p_i$  is the partial pressure for each of the reactants [15]. The equilibrium constant has the value of reaction quotient at equilibrium,

$$K = \Phi_{\text{equilibrium}}$$

from which it follows that the EMF is zero at equilibrium, as expected. At unit activity, which in the case of ideal gases means that all partial pressures are set to either one bar or one atmosphere, is assumed for the reaction (2-44) the reaction quotient becomes one and the Nernst equation simplifies to

$$E_r(T) = \frac{RT}{zF} \ln K(T) = E^0(T) \quad (2-46)$$

Unit activity is frequently referred to as *standard state* and  $E^0$  is therefore the *standard voltage* for the reaction at a given temperature. It is often pictured as an open circuit voltage. The standard voltage is more commonly expressed in terms of Gibb's free energy at standard state

$$E^0(T) = -\frac{\Delta G^0(T)}{zF} \quad (2-47)$$

Both the standard voltage and the Gibb's free energy at standard state can be found in tables for the reactions (2–39) and (2–40) [13, 16]. Taking all of the above into account the Nernst equations that corresponds to the two reactions are

$$E_{r,H_2\text{-reaction}}(T) = E_{H_2}^0(T) + \frac{RT}{4F} \ln p_{O_2} + \frac{RT}{2F} \ln \frac{p_{H_2}}{p_{H_2O}} \quad (2-48)$$

$$E_{r,CO\text{-reaction}}(T) = E_{CO}^0(T) + \frac{RT}{4F} \ln p_{O_2} + \frac{RT}{2F} \ln \frac{p_{CO}}{p_{CO_2}} \quad (2-49)$$

The oxygen partial pressure must be given in the same unit as the pressure in the tables for the standard state values, since the logarithmic term represents the pressure deviation from unity. Both reactions can take place at the same time in the fuel cell without limiting each other if the oxygen partial pressure at the cathode is held constant. In order to calculate the EMF that is generated when this occurs, it is necessary to consider how much of the free energy that each of the reactions stands for, in accordance with (2–42). This is proportional to the amount available of each reactant and calculated using a weighted average value. At the same time, it is possible to extract the oxygen partial pressure term from the above equations and consider the EMF to consist of three different contributions.

$$E_{r,H_2\text{-feed}}(T) = \frac{\kappa_{H_2}}{\kappa_{H_2} + \kappa_{CO}} \left( E_{H_2}^0(T) + \frac{RT}{2F} \ln \frac{p_{H_2}}{p_{H_2O}} \right) \quad (2-50)$$

$$E_{r,CO\text{-feed}}(T) = \frac{\kappa_{CO}}{\kappa_{H_2} + \kappa_{CO}} \left( E_{CO}^0(T) + \frac{RT}{2F} \ln \frac{p_{CO}}{p_{CO_2}} \right) \quad (2-51)$$

$$E_{r,O_2\text{-feed}}(T) = \frac{RT}{4F} \ln p_{O_2} \quad (2-52)$$

where  $\kappa_{H_2}$  and  $\kappa_{CO}$  are the molar fractions of the incoming fuel that consist of hydrogen and carbon monoxide respectively. The total EMF is the sum of the three equations and it can be modeled as a positive potential step that is introduced by the chemical reactions at the anode-electrolyte interface. Remembering this, it is important to change the sign in front of (2–52) when it is applied on the cathode side.

For the remainder of this chapter and the following chapters  $E_r$  will refer to the total EMF. The temperature dependence of the EMF will be regarded as implicit and the specifying parenthesis will therefore also be left out. [1, 13, 14, 17, 18]

#### 2.4.4 Cell Overpotential

The difference between the EMF and the actual cell voltage is referred to as the overpotential or total *polarization* of the cell. It can be divided into three different types of polarization: *activation*, *concentration* and *ohmic*.

Activation polarization arises due to an energy barrier, called activation energy, which the involved species must overcome in order for a chemical reaction to take place. The barrier arises when the reaction steps have varying rapidity. The polarization is the

extra potential necessary to make sure the slower steps do not influence on the desired rate. Generally there is one or more slow rate-determining steps that are dependent on temperature, pressure and electrode material. The activation polarization is in turn a function of the electrode reaction and the current density. In an SOFC, where the temperature is high, the reaction is fast and the activation polarization is usually small.

Concentration polarization is the voltage drop that follows from lowered concentration of the reactant species at the reaction site. This limits the rate of the chemical reaction. There are several factors that contribute to this polarization, for example slow diffusion through the pores of the electrodes, which makes the chemical reaction diffusion limited according to the discussion in section 2.4.2. Other factors are slow solution and dissolution of the reactants to and from the electrolyte as well as the diffusion through the electrolyte. At high operating temperatures the concentration polarization is usually low.

Ohmic polarization refers to the potential loss due to resistance to electric flow in the structure. This occurs both at contacts and for the electronic conduction in the electrodes, but mainly for the ionic conduction in the electrolyte. In order to reduce ohmic losses it is most efficient to either decrease the size of the electrolyte or to increase to the ionic conductivity. All ohmic losses obey Ohm's law and the ohmic polarization can therefore be expressed by

$$\eta_{ohm} = I(R_{anode} + R_{electrolyte} + R_{cathode} + R_{contacts}) = IR_{cell} \quad (2-53)$$

where  $I$  is the current through the cell and  $R_i$  is the resistance of each part. The resistance of the cell remains approximately constant as the current increases and the ohmic polarization therefore varies directly and in principal linearly, with the current. The resistance of the different components, which depends on the material and the type of conduction, will be further discussed in section 2.5.

Figure 2-2 is a principal sketch for the current-voltage characteristics in a fuel cell. It shows that each type of polarization has a region where it dominates the overpotential. In an SOFC where both activation and concentration polarizations can be assumed small a

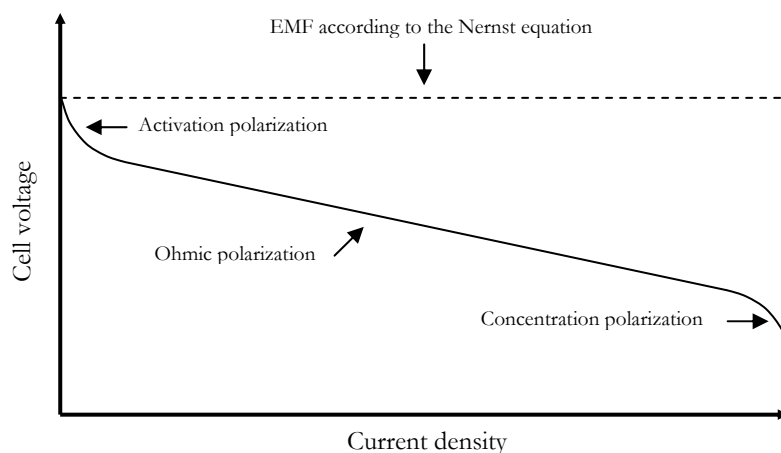


**Figure 2-2:** Fuel cell current-voltage characteristics [12].

good approximation is to estimate the overpotential as the ohmic polarization varying linearly with the current. This gives the actual cell voltage as

$$V_{cell} = E_r - \eta_{ohm} \quad (2-54)$$

[12, 13, 17]

### 2.4.5 Power Generation and Dissipation

The rate at which energy is converted from one form to another is called power, measured in J/s or the identical unit, W. One example is the dissipated power generated by ohmic resistance. It is energy transmitted from the electrical field to the structure in the form of thermal vibrations. Joule's law gives this as

$$P = V \cdot I \quad (2-55)$$

where  $V$  is the voltage and  $I$  the current. When this equation is formulated on point form it gives the power density measured in W/m<sup>3</sup> [19].

$$Q = \mathbf{E} \cdot \mathbf{j} \quad (2-56)$$

In the last expression  $\mathbf{E}$  represents the intensity of the electrical field and  $\mathbf{j}$  the current density, terms that will be further discussed in the following sections. The total net power generated by a cell is calculated by multiplication of the actual cell voltage with the current. If the assumption of an overpotential dominated by linearly varying ohmic polarization holds, in accordance with (2-54), the power can be expressed as

$$P_{cell} = IE_r - I^2 R_{cell} \quad (2-57)$$

where  $I$ ,  $E_r$  and  $R_{cell}$  represent the current, the EMF and the cell resistance as stated in the section above. The expression shows that the net power is the difference between the EMF generated power and the dissipated power and that the power-current variation is parabolic. The current that generates the maximum power is found by differentiating (2-57) with respect to the current. It is

$$I_{maximum\ power} = \frac{E_r}{2R_{cell}} \quad (2-58)$$

Inserted in (2-54) this value yields the following voltage

$$V_{maximum\ power} = \frac{E_r}{2} \quad (2-59)$$

[13]



## 2.4.6 Transformation of the Gas Compositions by Chemical Reactions

Due to the chemical reactions presented in section 2.4.1 the constitution of the incoming gases in the electrodes will vary along the interface to the electrolyte during operation. On both sides of the electrolyte the reactions involve transformation of charge carriers, which makes it possible to quantify the reaction rate in all points along the interface by using the scalar product of the current density  $\mathbf{j}$ , given in A/m<sup>2</sup>, with the normal vector  $\hat{\mathbf{n}}$ , defined as a vector of unit length perpendicular to the interface and pointing out of the electrode. By dividing this product with the number of electrons  $z$  that each oxygen molecule detaches when it is divided into two ions, and the amount of charge one mol of electrons contains, the number of consumed molecules per second in each point for the electrode reactions can be attained. At the cathode where every molecule supplies two ions and four electrons, the result becomes

$$\mathbf{n}_{O_2} = -\frac{\mathbf{j} \cdot \hat{\mathbf{n}}}{4F} \hat{\mathbf{n}} \quad (2-60)$$

This parameter has the dimension mol·s<sup>-1</sup>·m<sup>-2</sup> and represents the diffusion flux out of the porous cathode at the electrolyte border. The negative sign is included since it goes in the opposite direction to the current density. In order to conduct the same calculation for the process at the anode, it is necessary to decide the amount of ions that take part in each of the reactions (2-39) and (2-40). This can be done in accordance with the theory in section 2.4.2 with the assumption that reaction rates are much faster than the ion diffusion through the electrolyte. This gives that the equilibrium constant  $K$  for the fuel balance reaction (2-41) is very close to one. This shows that the relationship between the amount of water produced and carbon dioxide produced is directly related to the available amount of hydrogen and carbon monoxide.

$$\frac{[H_2O]}{[CO_2]} \approx \frac{[H_2]}{[CO]}$$

If the fuel mix is assumed to consist of ideal gases, the proportions between the production of water and carbon dioxide can be expressed using the supplied fuel molar percentage for hydrogen and carbon monoxide, in the same way as in section 2.4.2. Both reactions demands two electrons so the flux of water and carbon dioxide into the anode can be written as

$$\mathbf{n}_{H_2O} = -\frac{\kappa_{H_2}}{\kappa_{H_2} + \kappa_{CO}} \cdot \frac{\mathbf{j} \cdot \hat{\mathbf{n}}}{2F} \hat{\mathbf{n}} \quad (2-61)$$

$$\mathbf{n}_{CO_2} = -\frac{\kappa_{CO}}{\kappa_{H_2} + \kappa_{CO}} \cdot \frac{\mathbf{j} \cdot \hat{\mathbf{n}}}{2F} \hat{\mathbf{n}} \quad (2-62)$$

where  $\kappa_i$  represents the molar fractions in the gas that reaches the reaction site. In this case both the normal vector and the current point out of the electrode, and the negative signs are included since the production fluxes are going into the electrode. Naturally,

hydrogen and carbon monoxide disappears with the same rate as water and carbon dioxide are produced

$$\mathbf{n}_{H_2} = -\mathbf{n}_{H_2O} \quad (2-63)$$

$$\mathbf{n}_{CO} = -\mathbf{n}_{CO_2} \quad (2-64)$$

Hydrogen and carbon monoxide vanish at the anode-electrolyte border, and the fluxes are therefore opposite to those of water and carbon dioxide.

### 2.4.7 Heat Production from Chemical Reactions

When a chemical reaction takes place it generates heat that enters the surrounding system. The energy difference before and after the reaction is known as the reaction enthalpy  $\Delta H$  as mentioned in section 2.4.1 and the portion of it that turn into heat depends on the circumstances. In an electrochemical reaction such as at the interface between the electrodes and the electrolyte in a fuel cell, a large portion of the energy is generated as electrical energy and therefore available to extract work from at high efficiency. This is the Gibb's energy discussed in section 2.4.2. When all of it is converted into electrical energy the operation is said to be *reversible* and the heat generated can be written as the difference between the enthalpy and Gibb's energy. This gives

$$Q_{reaction} = -(\Delta H - \Delta G) \quad (2-65)$$

given in J/mol [13]. The negative sign is included since this concerns the heat absorbed by the fuel cell and not the heat generated. Unlike the Gibb's energy, the enthalpy has very little dependence on the pressure at high temperatures, which means that with a very good approximation the value for the enthalpy at standard state can be used. However, since this is not the case for Gibb's energy it is necessary to use the fact that Gibb's energy can be expressed in terms of Nernst equation when the pressure deviates from standard state. A combination of the terms given equation (2-42) to (2-47) yields

$$\begin{aligned} Q_{reaction} &= -\Delta H^0 + \Delta G = -\Delta H^0 - zF \cdot E_r = -\Delta H^0 - zF \cdot E^0 + RT \ln \Phi(T) = \\ &= -(\Delta H^0 - \Delta G^0) + RT \ln \Phi(T) \end{aligned} \quad (2-66)$$

The reaction heat can also be expressed in terms of *entropy*, a measure of to which extent a high quality form of energy has been degraded into a low quality form of energy. In this case it quantifies the transformation of chemical energy into thermal motion in the structure. The second law of thermodynamics states the following in reversible operation [14].

$$\Delta S = \frac{Q}{T} \quad (2-67)$$

With this taken into account, the reaction heat can also be written as

$$Q_{reaction} = -T \cdot \Delta S \quad (2-68)$$

The entropy at standard state can, for most reactions, be found in tables in the same way as for the Gibb's free energy [16]. The following equation that now can be derived is therefore useful.

$$Q_{reaction} = -T \cdot \Delta S^0 + RT \ln \Phi(T) \quad (2-69)$$

Naturally the heat that is generated differs depending on which of the two reactions (2-39) and (2-40) that occurs. Taking this into account yields

$$Q_{H_2-reaction} = -T \cdot \Delta S_{H_2}^0 - RT \left( \frac{1}{2} \ln p_{O_2} + \ln \frac{p_{H_2}}{p_{H_2O}} \right) \quad (2-70)$$

$$Q_{CO-reaction} = -T \cdot \Delta S_{CO}^0 - RT \left( \frac{1}{2} \ln p_{O_2} + \ln \frac{p_{CO}}{p_{CO_2}} \right) \quad (2-71)$$

As in the derivation of Nernst equation the proportions between the reactions can be decided using the molar fraction  $\kappa_i$ . At the same time it can be useful to take into account that this derivation so far has been looking only at the amount of heat generated per mol. In a model considering the electrode-electrolyte interface as being a line, the generated heat must be specified as a flow, given in  $J \cdot s^{-1} \cdot m^{-2}$ . This is realized by multiplying the derived heat generation above with the diffusion flux from equations (2-61) and (2-62), as given in the following

$$q_{reaction} = Q_{H_2-reaction} \cdot \mathbf{n}_{H_2O} \cdot \hat{\mathbf{n}} + Q_{CO-reaction} \cdot \mathbf{n}_{CO_2} \cdot \hat{\mathbf{n}} \quad (2-72)$$

which can rewritten to

$$q_{reaction} = -T \left[ \frac{\kappa_{H_2} \left( \Delta S_{H_2}^0 + R \ln \frac{p_{H_2}}{p_{H_2O}} \right) + \kappa_{CO} \left( \Delta S_{CO}^0 + R \ln \frac{p_{CO}}{p_{CO_2}} \right)}{\kappa_{H_2} + \kappa_{CO}} + \frac{R}{2} \ln p_{O_2} \right] \frac{\mathbf{j} \cdot \hat{\mathbf{n}}}{2F} \quad (2-73)$$

This is the reaction heat expression if all heat is assumed to be produced at the anode-electrolyte interface. To obtain the corresponding expression for the cathode-electrolyte interface the negative sign has to be omitted due to the direction of the current.

## 2.5 Electric Conduction in Ceramics

Charge transport in ceramic structures occurs as conduction that in general is both *ionic* and *electronic*. In order to decide which one of the two that dominates, the

transference numbers<sup>5</sup> of the species can be compared. For a solid oxide fuel cell to function it is necessary that the relative magnitude of ionic transference number is very large in the electrolyte and vice versa for the electronic in the electrodes. This is the case for all typical SOFC materials and for these materials the electronic conduction in the electrolyte can, as well as the ionic conduction in the electrodes, be neglected without losing noticeable accuracy. The parameter that describes the degree of conduction is called conductivity and measured in  $\text{A V}^{-1}\cdot\text{m}^{-1}$  or  $\text{S}\cdot\text{m}^{-1}$ . The inverse of the conductivity is known as the resistivity and consequently it is the degree of resistance. The following three sections present the theory of conduction in ceramics and how to model it with mathematics.

### 2.5.1 YSZ

Electric conduction in a ceramic material depends on its lattice structure and defects. In yttria-stabilized zirconia, YSZ, ionic conduction occurs due to high oxygen-ion vacancy, which in turn gives good oxygen-ion mobility. The defect structure can however be modified by changing the oxygen partial pressure, but this also affects the electronic conduction and not only the ionic. The electronic conduction in ceramics is a type of semi-conduction and the charge carriers can be either electrons or holes<sup>6</sup>. For low pressures the YSZ display the same type of conduction as n-type semiconductors whereas high pressures causes the material to display p-type behavior<sup>7</sup>. At intermediate pressures the concentration of vacancies is not dependent on the partial pressure, but instead fixed by the yttria dopant<sup>8</sup> level. In this pressure range the concentration of electrons and holes are about the same and if then dopant level exceeds these concentrations the conduction becomes ionic.

Apart from the oxygen partial pressure the conduction is also dependent on the temperature. A higher temperature gives more vacancies and better conduction. For YSZ with dopant levels between eight and ten molar percent of yttria this means that the conduction can be regarded solely ionic at temperatures between 800-1000°C.

In order to use YSZ in applications where it is supposed to have electronic conduction independent of, or in the intermediate region of the oxygen partial pressure, it is necessary to mix it with a metal. This must also be done to achieve high enough electronic conduction to obtain a useful electrode material. In SOFC applications nickel is the most common choice, as mentioned in earlier sections. The conductivity of the cermet is highly dependent on the amount of metal. In the mixture different conduction mechanism occur that can transport charge through the structure, one ionic path originating from the YSZ as described above and one electronic path through the nickel phase. There is a threshold for the nickel content in the mixture at about 30 percent of the volume. Under this value the conduction is mainly ionic and in the same order as for

---

<sup>5</sup> The transference number is defined as the ratio of a certain species' contribution to the conductivity to the total conductivity.

<sup>6</sup> Terms such as "holes", "n-type", "p-type" and "dopant" are typical for semi-conductor theory. This theory and its terminology will not be presented in further detail in this report. It is included as a brief background to the approximations made regarding the electric conduction in the modeling work. A more thorough explanation falls outside the scope of the thesis. For further reading, see [13].

<sup>7</sup> See note 6.

<sup>8</sup> See note 6.

regular YSZ. Above this value the electronic conduction becomes possible and the conductivity becomes roughly three orders of magnitude greater. [13]

### 2.5.2 LaMnO<sub>3</sub>

Oxides with the general formula ABC<sub>3</sub> have a certain structure that has proved to be very useful as cathode and interconnect material in SOFC applications. The electric conduction in LaMnO<sub>3</sub> is considered to be of p-type and due to the 3d valence<sup>9</sup> electrons. Doping with acceptor<sup>10</sup> ions is frequently used to enhance the conductivity. For this purpose strontium is the most common choice today. Under some conditions LaMnO<sub>3</sub> also displays ionic conduction because of oxygen vacancy formation, in the same ways YSZ does. However, the electronic conduction is substantially greater, especially when the material is doped. [13]

### 2.5.3 Mathematical Description

According to the principle of conservation of charge, electric charge may not be created nor destroyed. This means that the amount of charge in a closed region always remains the same unless there is a net flux going in or out of the region. In the case of electrochemical reactions in fuel cells, this means that an equal amount of charge must be carried to and from the reaction zone. Since no other current sources are present this means that the electric current becomes steady and divergenceless so that the equation of continuity can be written as

$$\nabla \cdot \mathbf{j} = 0 \quad (2-74)$$

where  $\mathbf{j}$  is the current density, with no difference regardless if the conduction is ionic or electronic. Both types of current are also governed by Ohm's law, which can be expressed in several ways. On point form it relates the current density to the electric field  $\mathbf{E}$  via a material and temperature dependent proportionality constant  $\sigma$ , which is the conductivity that was discussed in the two previous sections, in the following way

$$\mathbf{j} = \sigma \mathbf{E} \quad (2-75)$$

The electric field intensity is a fundamental quantity in electromagnetic theory and can be seen as the force a unit charge experiences when it is placed in the field. It can be measured in N/C, but is more commonly given in V/m. Since vector quantities can be difficult both to handle and determine, the prevalent method is to define a scalar electric potential  $V$  in accordance with

$$\mathbf{E} = -\nabla V \quad (2-76)$$

and use this as the free variable in the region that is to be modeled. A combination of the expressions above gives the following equation to solve

---

<sup>9</sup> See note 6.

<sup>10</sup> See note 6.

$$\nabla \cdot (-\sigma \nabla V) = 0 \quad (2-77)$$

By applying and solving this expression for the different parts of the fuel cell the electric profile can be received. However, considerations to the type of conduction, temperature and material must be done by inserting proper values for  $\sigma$  in each region and linking these regions together with boundary conditions. [19]

## 3 Femlab

Femlab is a Matlab based computational software supported by a graphical user interface that facilitates model programming. This chapter presents some of Femlab's specific features, and its working methodology as well as considerations made when creating the SOFC model.

### 3.1 The Software

One of the main reasons why Femlab was chosen for the implementation of the Rutquist cell was the graphical user interface and the flexibility of the “*multiphysics*” modes. The expectation was that it would be both easy to work with and powerful. That view slightly changed during the project. The software will be presented from the perspective of a first time user. Further evaluation and conclusions can be found in chapter five and six. The first section of this chapter however, examines the structure of the software and the graphical user interface.

#### 3.1.1 Introduction to Femlab

Femlab is marketed as an engineering tool based on partial differential equations for multiphysics modeling in the Matlab environment. The term multiphysics encompasses the ability to model several physical phenomena as well as chemistry and generalized differential equations. The software uses finite element methods, and the utilization and creation of a computational mesh is an integrated part in the software design. There are many ways in which one can work with Femlab. The most common is to use the graphical interface, and program the models that way. Another option is to use the m-file system in Matlab. The m-files are batch-files that execute a sequential list of entered commands. It is in this way possible to define geometries and call on the computational modules in Femlab from the Matlab command prompt. This offers good control but is tedious. In addition, models can also be programmed in the so called equation mode where the governing relations are implemented by defining mathematical expressions.

Once a solution is attained, the data can be presented in a variety of ways, e.g. in two or three dimensions and as contour or cross section plots. The software offers many ways to handle the solution data with post-processing functions.

#### 3.1.2 The Femlab Module System

One of the strengths with Femlab is that the software is module based. This is an advantage when additional functionality is needed, and when programming models containing several different physical phenomena. The system offers good flexibility, as the user can buy new modules when needed. Each module contains several modes that are more or less specialized for modeling certain processes or phenomena. As an example was the Chemical Engineering Module used in this project. Since the modes can be used independently this offers good flexibility.

Femlab automatically generates the variables needed for the different modes which facilitate the programming. The modes can be used to perform simultaneous calculations with different initial conditions and parameters. They are independent and can be used

individually but the quality of the module based system lies in the interconnectivity. The free variable in one mode can be used as input in another, e.g. the gas temperature in the SOFC model was used both as input in the in the Darcy law mode, to determine the gas density, and in the heat transfer modes as a coupling between the gas and the structure.

## 3.2 Work Procedure

In this section the design and the user interaction with Femlab will be discussed. The software can be used in several alternative ways.

### 3.2.1 The Graphical User Interface

As it has been previously mentioned Femlab uses a graphical interface for controlling the programming, and through this it offers an instrument for easy implementation of different calculation modes. Geometries can be drawn directly in the program in one to three dimensions. This offers an advantage over other programs using command-line coding.

However, Femlab also offers a system for user dialogue that makes it possible to numerically define the geometries. The user interface is unfortunately not always logical and the Windows standards for dialogue boxes are not fully implemented. Especially the lack of support for standard keyboard commands makes the work more time consuming than necessary.

### 3.2.2 Methodology

There is a clear sequential order in which the model programming should be done. The first thing to do is to define a geometry, and the second is to apply modes or equations to the different domains of the geometry. If the geometry is divided in parts these are called *subdomains* and the mode in which you define the governing relations is consequently named *Subdomain Mode*. Here are also the initial conditions defined. Constants and expressions that are used frequently can be made available globally in the model. This allows more efficient programming and better code legibility.

Third, entering the *Boundary Mode* the conditions on the border of the different subdomains are set. It is possible to use expressions that involve input from other modes and subdomains. In the *Mesh Mode* the user can adjust the mesh in order to get more accurate and precise results. The adjustments of the Mesh Mode can normally be omitted since Femlab automatically generates a mesh from the standard settings. Finally, the user decides how to solve the problem and if it is a time-dependent problem, also the start and stop times along with the time resolution. The different solvers offer numerous possibilities for adjusting the solution process. This is important in order to make sure that the solution converges. The three main solution types are: linear, non-linear and non-linear time-dependent.

Having acquired a solution, the data can be presented in various ways by applying different plot types. The option to use mathematical tools to evaluate the data is very useful and, for example, is integration of the studied variables around edges and over subdomains possible. Mathematical expressions can also be entered to look at different aspects of the data.



### 3.3 The SOFC Model

This section deals with the implementation of the Rutquist design in Femlab, and the challenges faced. It starts off with how the geometry was chosen, and continues with a discussion on the different modes used in the model.

#### 3.3.1 Implementing the Unit Cell

The amount of computation needed to solve a problem is always a primary concern using numerical solvers. There are however, several ways of reducing the complexity. One efficient method is to decrease the number of nodes defining the mesh and another is to search for symmetries. The first step when defining the unit cell was to look for the smallest possible geometry that contained all relevant data and then identify symmetries in this geometry. More on how the actual cell was chosen can be found in conjunction to the description of the unit cell, section 4.1.2.

It soon became apparent that due to the large scale difference between the vertical and the horizontal directions of the geometry, the automatically generated mesh created a vast number of nodes that brought the total number degrees of freedom close to twenty thousand. This naturally created very large and time demanding computations that made the model difficult to work with. The mesh parameters that can be adjusted unfortunately only allow refinement of the mesh, and since the automatic generator strives for creating equilateral triangles, the geometry in itself made it impossible to reduce the problem to manageable proportions. The solution was to scale the vertical direction so that the geometry became close to squared and then make the calculations on the original sized problem over night.

#### 3.3.2 Implementing the Multiphysics

The SOFC modeling work required that many different physical phenomena were taken into consideration and accounted for. The implementation in Femlab made use of the standard modes available and also modes from the Chemical Engineering Module. The different modes were then coupled to each other allowing for the simulation of the cross dependent processes. Many of the gas parameters, for example the heat capacity and the density, depend on the temperature and hence create a link to the temperature mode. This interlinking increased the complexity of the problem and also probably affected the convergence of the solution. Strong feedback loops tend to have an adverse effect on the chances of finding a solution.

In many cases the parameters used in the Femlab modes had to be calculated using external models and this was partly done in Matlab and partly by defining expressions in Femlab. The Matlab functions were then called on from Femlab.



## 4 SOFC Model

This chapter describes implementation of the Rutquist cell in Femlab and looks at both the theoretical as well as practical considerations that had to be made. Part one discusses the assumptions made regarding input parameters and the concept of the unit cell whereas the second section studies the different modes and how they were implemented.

### 4.1 Modeling the Structure and Basic Conditions

A large number of parameters have to be taken into consideration in order to model a fuel cell system. This section starts with an analysis of the composition of the incoming gases that were assumed to originate from a fuel processor. Using relevant data for the incoming gas was essential in order to build a model producing accurate results. For the same reason the properties of the materials in the structure had to be modeled appropriately. Equally important was to have good knowledge of the modeled structure and its function. These matters are also discussed below.

#### 4.1.1 The Fuel Processor

A catalytic *autothermal reformer* (c-ATR) can be used to convert liquid fuel to gas. If diesel is assumed to be the onboard fuel, the c-ATR will create a gas mixture consisting of H<sub>2</sub>, CO, CO<sub>2</sub>, and N<sub>2</sub> with small amounts of CH<sub>4</sub>. Since steam is present in this process there will also be water present in the mixture. The assumed gas composition in the fuel channel is presented in Table 4–1. Four different articles treating fuel processing were compared [2, 10, 20, 21] and the values were found as typical in a wide range of possible compositions. The working temperature for a c-ATR ranges from 750 to 850°C, so the temperature of the inflowing gas was set to 1073 K. In view of the fact that this is the same operating temperature as the SOFC stack has, it would be possible to thermally integrate the reformer and the fuel cell stack, which however was not within the scope of the thesis. The inlet air was assumed to be taken from the surrounding and therefore of standard composition, although somewhat simplified. The air composition is presented in Table 4–1 as well.

**Table 4–1:** *Air and gas channel composition.*

Gas channel composition						Air composition	
H <sub>2</sub>	CO	H <sub>2</sub> O	CO <sub>2</sub>	N <sub>2</sub>	CH <sub>4</sub>	N <sub>2</sub>	O <sub>2</sub>
50 %	25 %	12 %	6 %	6 %	1 %	79 %	21 %

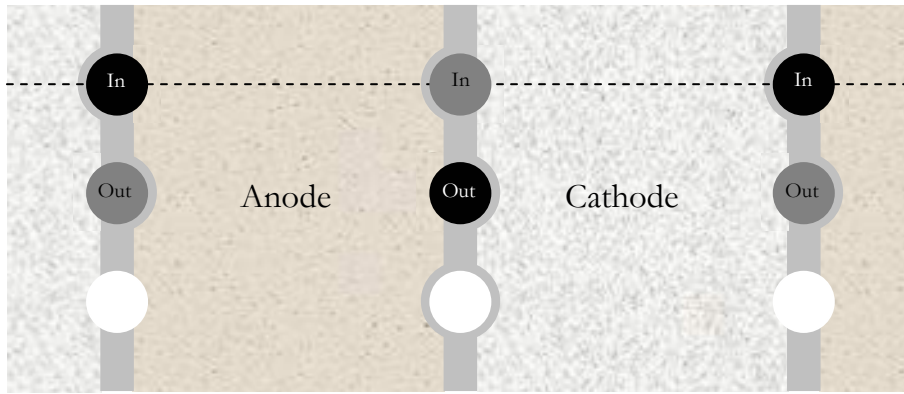


**Figure 4-1:** Schematic view of a portion of an arbitrary cross-section in the SOFC structure developed by Volvo Technology Corporation. The black circles show the fuel gas channels and the grey the air channels that lead from top to bottom in the stack. The white circles are interconnects that lead the current from left to right in the picture. The lighter grey sections are ion-conducting electrolyte. Since the electrolyte is not porous, the gas mixtures from the channels diffuse from the channels marked “In” to the channels marked “Out”. The dotted line represents the intersection with the cross-section presented in figure 4-2. It can be noticed that the main diffusion direction does not coincide with the dotted line.

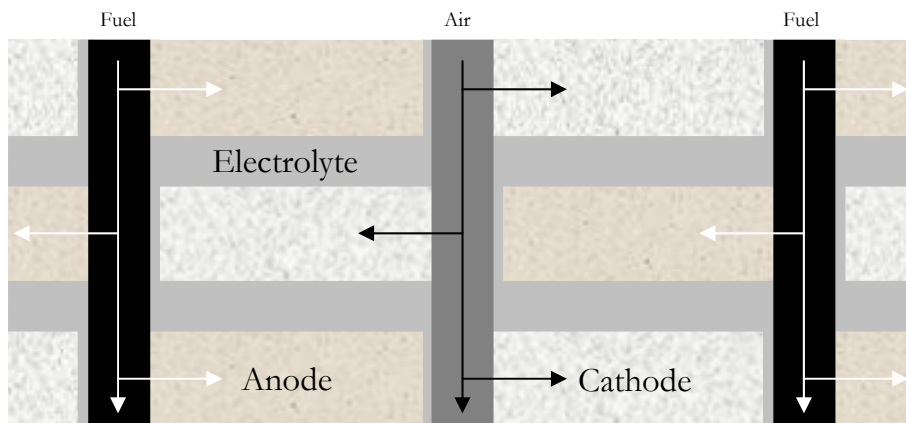


**Figure 4-2:** Three layers side view of the same structure as seen in the previous figure. Fuel and air flows through the channels and diffuses into the porous anode and cathode respectively. At the electrode-electrolyte-interfaces chemical reactions generate ion and electrons that produce a current. It goes from left to right and from the anodes to cathodes through the electrolyte layers.

#### 4.1.2 The Original Structure and the Unit Cell

In ordinary SOFC solutions the fuel and the oxygen reaches the *triple phase boundary*<sup>11</sup> by permeating the electrodes from the bottom and the top respectively. This is not the case in the idea presented by Rutquist at Volvo Technology Corporation. Instead of being parallel, the triple phase boundaries and the gas channels are perpendicular, and the permeation through the electrodes therefore occurs laterally. The gas channels lead from top to bottom in the stack while the current goes from left to right, except when it passes

<sup>11</sup> The triple phase boundary refers to the surface where the electrolyte meets the porous electrode. The permeated gas meets two different solid structures in the same point.

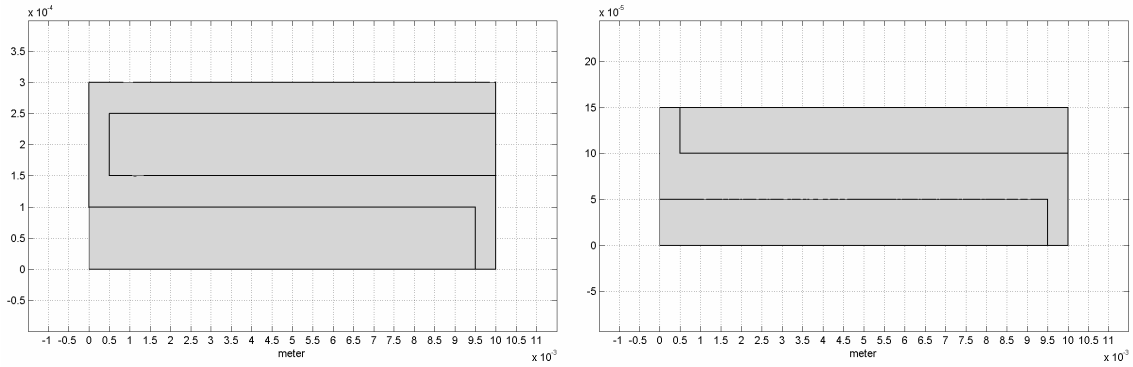


**Figure 4–3:** Unit cell geometry (Subdomain mode in FEMLAB).  
*Preliminary version to the left and final version to the right.*

through the electrolyte where it goes either up or down to another layer. Viewed from above each layer consists of stripes with anode and cathode material separated by isolating material, gas channels and interconnecting material arranged in a repeated pattern as showed in Figure 4–1. Gaseous fuel from the converter and air are fed into certain ingoing channels from where they then diffuse through the electrodes and reach outgoing channels. Air is fed to the cathode and fuel gas to the anode.

During normal operation of the SOFC stack chemical reactions take place along the electrolyte-electrode-interfaces that consumes hydrogen, carbon monoxide and oxygen. This creates an electromotive force that, when the stack is externally loaded, gives rise to a current through the structure. In the electrolyte the charge carriers are oxygen ions while the conduction is electronic through the anode and the cathode.

The first step in the modeling work was to create a simple geometry in Femlab, consisting of a two-dimensional unit cell, designed to correspond to the original Rutquist cell. With the cross-section given in Figure 4–2 as a starting point, the unit cell was modeled to be the smallest element possible that by repetition could reproduce the whole structure. Figure 4–3 shows the unit cell in its original configuration in Femlab with the almost s-shaped electrolyte surrounding the cathode and with the anode in the bottom. The electrolyte material was set to be YSZ while  $\text{LaMnO}_3$  was chosen for the cathode and a 30 percent Ni/YSZ cermet for the anode. They are all standard SOFC materials in accordance with the theory in section 2.1.

The height of the unit cell was decided to by summing the typical thicknesses of the different layers in ordinary cell designs [12], and therefore also within the range of what is possible to produce in reality. The electrolyte thickness was set to  $50\ \mu\text{m}$  both for the layer above and under the cathode. The anode and the cathode were in the same manner specified to be  $100\ \mu\text{m}$  thick. The width had already been specified in the original idea to be ten millimeters and from this a preliminary unit cell was drawn as seen to the left in Figure 4–3. It contained two electrolytes and two full sized electrodes. However, as can be seen in same figure, when this unit cell was repeated in both the downward and upward directions it was symmetric and could therefore be simplified further by removing one of the electrolytes and cutting both electrodes in half. This gave the final version of the unit cell as showed to the right in Figure 4–3,  $150\ \mu\text{m}$  thick and ten millimeters wide.

**Table 4–2:** *Material parameters in the unit cell valid at 1073 K.*

	Ni/YSZ cermet	YSZ (8 mol%)	LaMnO <sub>3</sub>
Component	Anode	Electrolyte	Cathode
$C_p$ – specific heat capacity [J/(kg K)]	1054	1126	960
$k$ – thermal conductivity [W/(m K)]	28	2	4
$\sigma$ – electric conductivity [1/( $\Omega$ m)]	$5 \cdot 10^4$	10	$1.6 \cdot 10^4$

In addition to this the width of the gas channels also had to be considered. They were set to be two millimeters wide, giving each a radius of one millimeter on both sides of the unit cell that had to be included for each unit cell when the size of a complete stack were to be calculated.

### 4.1.3 Material Parameters

A search for material parameters was conducted and since the amount of data available turned out to be limited, it became time demanding even though that the outcome was sparse. The values sought were supposed to be valid at and around the temperature of operation, 1073 K. In some cases no values at all were found, or values in the wrong temperature domain, and approximations had to be made. Especially the specific heat capacities for the different parts of the structure were difficult to find. For the Ni/YSZ cermet the specific heat capacity and the thermal conduction were calculated with linear interpolation between nickel and yttria stabilized zirconia. The specific heat capacity for the LaMnO<sub>3</sub> was approximated by using the value for manganese (Mn), which agrees well with other oxides and ceramics of the same type. All the tabulated specific heat parameters were given for room temperature and in order to compensate for the change with temperature up to the operational region they were multiplied by a factor two. Roughly this corresponds to the development with temperature for similar types of ceramics.

Regarding the electric conduction it must be noticed that the values for the electrodes was found to differ from the value of the electrolyte by a couple of magnitudes. This is due to fact that the charge carriers are different in the electrodes than in the electrolyte, as discussed in section 2.5. In the Table 4–2 the values of the thermal capacity, the specific heat capacity and the electric conduction are given for the three chosen materials. More material parameters and references for all values can be found in Appendix A.

### 4.1.4 Gas Parameters

The gas parameters necessary for the model were calculated using tabulated values for thermodynamic and transport properties from literature [9]. Experimental data had been assembled from several different measurements and complemented by validated estimation in order to bring about the temperature dependency of a number of gas properties in the form of sixth order polynomial curve fits for all gases of interest in the modeling work. The coefficients used were noted as valid in the range 273-1473 K.

The parameters sought and calculated from the polynomial coefficients were the thermal conductivity  $k$ , the molar heat capacity  $C_p$ , the density  $\rho$  and the binary diffusion

coefficients used in the Maxwell-Stefan diffusion mode that will be discussed further in section 4.3.5. The compositions of the gas mixtures in the fuel and air channels were set to the values given in Table 4–1 and assumed to consist of ideal gases. This meant that parameters for the mixtures could be calculated using a weighted mean of the included species. For example, the molar heat capacity was calculated as

$$C_p(T) = \sum_{i=1}^n \kappa_i \cdot C_{pi}(T) \quad (4-1)$$

where  $\kappa_i$  and  $C_{pi}$  represents the mole fraction and the heat capacity for the  $i$ :th species [9]. All parameter values were calculated using Matlab and implemented as functions in Femlab.

## 4.2 Bringing the Structure to the Temperature of Operation

When the model work had reached this point the next step was to apply the preferred modes on the two-dimensional Femlab unit cell and model the heating process. The basic assumption was that the high temperatures of the gases also could be used to heat the structure into Active Mode. Mainly heat transfer between the gas and the solid structure in the porous electrodes were presumed to achieve this, but also convection in the gas channels. Since, in all types of high-temperature fuel cells, it is very difficult to install an external heating system, this is probably the most efficient way to heat the structure. As soon as the cell has reached operational mode, the gas flows are instead cooling the structure and prevents it from getting too hot.

### 4.2.1 Heat Transfer Modes

In the Rutquist SOFC design heat transfer has to be considered and modeled in all parts of the unit cell. More specifically this meant within the solid structure, across the electrode-electrolyte interfaces, within the gas, to and from the gas diffusing in the electrodes and between the gas in the channels and the channel walls.

The heat distribution in the SOFC structure depends on the influence on the above mentioned processes. When implementing this in Femlab, the “Heat Transfer” mode was used for describing the temperature distribution in the solid structure while the “Conduction and Convection” depicted the situation in the gas mixture diffusing through the electrodes. These two modes were then linked to each other using the source terms. The heat transfer from the gas channels only shows up as a boundary condition in the Heat transfer mode and will be treated in the next section.

$$\rho C_p \frac{\partial T_s}{\partial t} - \nabla \cdot (k \nabla T_s) = Q_s \quad (4-2)$$

$$\rho C_p \frac{\partial T_g}{\partial t} + \nabla \cdot (-k \nabla T_g + \rho C_p T_g \mathbf{u}) = Q_g \quad (4-3)$$

The first equation is the ordinary heat transfer equation that governs the temperature distribution in the solid while the second is the combined conduction and

convection-equation that models the temperature in the gas. Terms denoted with an  $s$  refers to the solid, for example  $T_s$  that is the temperature in the solid structure, while terms denoted with  $g$ , such as  $T_g$ , describes the gas. Moreover, the density  $\rho$ , the specific heat capacity  $C_p$  and the thermal conductivity  $k$  refer to material parameters for the structure in the first equation and to the gas parameters in the second equation<sup>12</sup>. The coupling, in form of the source terms, was implemented as

$$Q_s = H(T_g - T_s) \quad (4-4)$$

$$Q_g = -Q_s \quad (4-5)$$

In accordance with the theory in section 2.3.3 this was modeled with a convective relation. The constant was evaluated through modification of a tabulated coefficient used for normal forced convection by compensating for the area of the pores per volume,

$$H = \frac{6}{\varepsilon d_p} b \quad (4-6)$$

with  $b$  denoting the forced convection coefficient,  $d_p$  is the pore diameter and  $\varepsilon$  the porosity. The pore diameter  $d_p$  was set to 1  $\mu\text{m}$  and the porosity  $\varepsilon$  to 0.3 in both electrodes, based on typical values from literature [3]. The forced convection coefficient was approximated to be 100 W/(m<sup>2</sup> K) in both electrodes, using tabulated values for air [5].

The structure was assumed to start at room temperature, 293 K, while the gas entering the gas channels and diffusing through the electrodes was set to 1073 K. The heating was assumed to be completed when the whole the unit cell had reached a temperature of at least 1023 K. This limit was regarded as the lower boundary of the Active Mode.

Since the unit cell was made symmetric, the upper and lower horizontal boundaries were set to symmetry in the Heat Transfer mode. In the Conduction and Convection mode the inlet gas boundaries were set to 1073 K, while the outlets were set to “convective flux”. This means that the convection contribution was assumed to be a lot larger than the conduction on these boundaries.

#### 4.2.2 Heat Convection from the Gas Channels

The next step was to analyze the thermodynamic behavior of the given geometry with heating from the gas channels at the sides included. The Reynolds number for the flow in the gas channel was assumed to be low enough for laminar flow.

According to theory, the heat in the gas channels is transferred to the surface of the ceramic unit cell by forced convection through a laminar film [13]. Equation (2-30) was used in order to estimate the film coefficient. The thermal conductivity was calculated in the same way as stated in 4.1.4 but as a function of the film temperature instead of the inlet gas temperature, in accordance with section 2.3.3. The independent variable of the heat transfer mode  $T_s$ , was used as the wall temperature and the inlet gas temperature of 1073 K was set to be the channel temperature. The width of the film was determined

---

<sup>12</sup> This has not been denoted in equations (4-2) and (4-3) because of its consequences for the legibility.



using equation (2–35) with  $Nu = 3$  and the gas channel diameter set to two millimeters, as stated in 4.1.2. This Nusselt number was found as typical and in accordance with several scientific articles [10, 11].

$$d_f = \frac{d}{Nu} \approx 6.67 \times 10^{-4} \text{ m}$$

### 4.2.3 Gas Diffusion in the Electrodes

The gas diffusion in the electrodes is, as mentioned earlier, important for the understanding of the temperature distribution in the cell, as well as for several of the features in the Active Mode model. However, this will be treated further in section 4.3.

The boundary conditions applied to the flowing gas were set in the form of pressures: two atmospheres at the inlet and one atmosphere at the outlet. Consequently the process was regarded as pressure driven and it could, for example, have been modeled using the Dusty Gas Model as described in the theory section. Due to time considerations and difficulties in implementing this model in Femlab, a mode based on Darcy’s law was instead chosen. It solved equation (2–4) under the assumption that the gas mixtures in the electrodes could be seen as homogeneous, and hence, that the binary diffusion played a minor role in the mass transfer. This approximation is acceptable in the Heating Mode, but not in the Active Mode and it will be discussed more in section 4.3.5.

In order to model the diffusion coefficient in (2–4), some modifications had to be made. Parameters were available only for the Knudsen diffusion constant and it was therefore used as presented in (2–19). As stated in section 4.2.1, the pore diameter and porosity was set to the values  $1 \mu\text{m}$  and  $0.3$  [3]. The tortuosity  $\tau$ , was set to  $0.5$  in both electrodes on the same basis [3]. The coefficient was then modified to suit the Darcy law mode by division with the pressure.

$$\frac{k}{\eta} = D_{iM}^e \frac{1}{p} \quad (4-7)$$

In order to approximate the efficient molar mass, an interpolation method was used where the molar masses of the different gases were weighed according to their fraction in the gas mixture.

## 4.3 Implementing Active Mode

When the structure had been heated to working temperature the next step was to implement the features in the operational mode. It was set off with some general assumptions.

### 4.3.1 General Assumptions

The model developed to analyze the heating procedure was used as the foundation for the model of the Active Mode. However, to begin with the electrical modes were developed separately and how this was done will be further described in the next section.

The solver was switched to steady-state solution and as initial condition the temperature was set to 1023 K in all parts of the structure, since this earlier had been determined to be the ignition temperature for the chemical reactions. The chemical reactions were assumed to generate both an EMF and heat, in accordance with the theory in section 2.4. Different outer loads were then modeled as connect between the anode and the cathode by varying the cell voltage. In combination with a chemically generated EMF the outer connection via the load brought about a direct current in the structure, driving electrons through the anode and the cathode, and ions through the electrolyte, as earlier described. In addition to this, heat was generated from ohmic losses. In order to model the EMF in Femlab two electric modes had to be introduced: one describing the electronic conduction in the electrodes, and one the ionic conduction in the electrolyte.

### 4.3.2 Electric Conduction Modes

The modeling of the electric conduction was made in accordance with section 2.5.3. The conduction was assumed to be solely electronic in the electrodes and solely ionic in the electrolyte. In Femlab two separate ‘‘Conductive Media DC’’ modes that solve equation (2–77) were chosen and implemented in the different regions of the unit cell. The first mode was set to model the electronic conduction and applied to the electrodes with the constant values for the conductivity in accordance with section 4.1.3. The second mode was applied only to the electrolyte in the same manner to model the ionic conduction. In these Femlab modes it was possible to specify the conditions on the boundaries by entering a value for the either electric potential or the inward current density. As a special option it was also possible to set the current to zero, meaning that there is symmetry or insulation.

The next step was to couple the two modes by setting appropriate conditions on the unit cell internal borders. This was done with the theory in section 2.4.2 as a starting point. A proper model had to contain both the potential steps introduced by the EMF at the electrode-electrolyte interfaces predicted by Nernst equation and a coupling of the current across the interfaces. The total EMF was implemented in two parts. One at the anode-electrolyte interface, where the partial pressure of the fuel components were available, using the sum of (2–50) and (2–51), and the other at the cathode-electrolyte interface, where the oxygen partial pressure was available, using equation (2–52).

On the two lines constituting the internal border between the anode and the electrolyte the following expression was set to be the electric potential in the ionic conduction mode.

$$V_{electrolyte} = V_{anode} + E_{r,anode} \quad (4-8)$$

with the EMF calculated as

$$E_{r,anode} = \frac{\kappa_{H_2} \left( E_{H_2}^0(T) + \frac{RT}{2F} \ln \left( \frac{p_{H_2}}{p_{H_2O}} \right) \right) + \kappa_{CO} \left( E_{CO}^0(T) + \frac{RT}{2F} \ln \left( \frac{p_{CO}}{p_{CO_2}} \right) \right)}{\kappa_{H_2} + \kappa_{CO}} \quad (4-9)$$

And on the lines forming the cathode-electrolyte border, the potential step caused by the EMF that was added to the electric potential looked like

$$E_{r, cathode} = \frac{RT}{4F} \ln p_{O_2} \quad (4-10)$$

In order to obtain the correct EMF over the electrolyte this value had to be subtracted when implemented on the cathode side,

$$V_{electrolyte} = V_{cathode} - E_{r, cathode} \quad (4-11)$$

The values for  $E^0$  were taken from second order polynomial curve fits made in Matlab to experimental data in the interval 900-1300 K according to a computer program called CEA, developed by the NASA Glenn Research Center<sup>13</sup>. The curve fits are presented in Appendix B. To simplify and speed up the Femlab calculations, the logarithmic functions were approximated with curve fits as well, using a third order polynomial for an appropriate interval around unity. This is presented in Appendix C. The partial pressure was calculated by multiplying the pressure from the Darcy law mode with composition of the gas mixture, given by the molar fraction in each point. The different methods to model the consumption of the reactants, including its effect on the pressure, are discussed in section 4.3.6. Due to difficulties and malfunctions in Femlab's resetting functions some versions of the Active Mode model file was made with the pressure approximated as a one-dimensional linear function instead of using the Darcy law mode. This had been concluded to be a very good description of the pressure profile from the results in the heating model.

However, this was not enough to build a complete electric model. As mentioned above it was also necessary to apply a current coupling between the different conduction modes. Since the boundary settings in the ionic mode had been used to model the EMF potential step, this had to be made in the electronic mode. The current densities were set equal in the adjacent subdomains with the expressions

$$\hat{\mathbf{n}} \cdot (\sigma_{anode} \nabla V_{anode}) = -\sigma_{electrolyte} \cdot \frac{\partial V_{electrolyte}}{\partial y} \quad (4-12)$$

at the horizontal anode-electrolyte interface, and

$$\hat{\mathbf{n}} \cdot (\sigma_{anode} \nabla V_{anode}) = -\sigma_{electrolyte} \cdot \frac{\partial V_{electrolyte}}{\partial x} \quad (4-13)$$

at the vertical anode-electrolyte interface. The same formulations were also used at the cathode-electrolyte interface, but without the negative signs in order to define the correct current direction. The two expressions above are stated as they had to be implemented in

---

<sup>13</sup> "CEA" stands for Chemical Engineering with Applications and "NASA" for National Aeronautics and Space Administration. The CEA computer program calculates chemical equilibrium compositions and properties of complex mixtures by association with independent databases that contain transport and thermodynamic properties of more than 2000 individual species. For more information, see [16]

Femlab, and it can be noticed that the current density is written in accordance with the theory in section 2.5.3, with  $\hat{\mathbf{n}}$  representing the normal vector. The easiest way to achieve the corresponding value for the left hand side of the expressions was to use the partial derivatives of the potential in the opposite direction to  $\hat{\mathbf{n}}$ . As it has been pointed out in several parts of this report this type of derivative coupling caused difficulties for the solver, but not to any damaging degree when it only concerned these couplings in the electric modes. Nevertheless, a large effort was made to find alternative formulations to the one presented in this paragraph. In this search it was found that Femlab solves the problem to the correct solution also when the current density in the electronic modes are set to isolation. This is a strange result whose explanation lies outside the scope of this thesis.

At this stage in the modeling work it could be established that the ohmic part of the overpotential had been implemented simply by using the theory presented in 2.5.3. The formulation naturally accounts for the potential lost due to the resistance in the structure since it uses the conductivity to calculate the electric field in each point. However, the results produced from the model at this stage did not account for activation or concentration polarization. They were both assumed small enough to be neglected. While this can be regarded as a good approximation for the activation polarization, it quickly becomes incorrect for the concentration, if not enough gas is supplied to the triple phase boundary. A proper model for the consumption of reactants, which will be further discussed in section 4.3.5, was intended to take care of this problem.

### 4.3.3 Stack Size and Power Generation

In order to determine the relationship between the stack size and the total power generated by the stack, it was necessary to establish circuit models for the unit cell as well as the stack. They were then used together with the equations presented in section 2.4.5. However, since the unit cell was modeled as two-dimensional some modifications had to be made. Since the dimension of the current density  $\mathbf{j}$  is  $\text{A}/\text{m}^2$ , the assumption was made that the unit cell has an infinitesimal width  $d\zeta$  in the third dimension, in order to calculate the total current. Then, when the contributions to the current from all points along either of the lines that constitutes the electrode-electrolyte interfaces in the unit cell was summarized, the following expression gave the current through the electrolyte in the thin plane

$$I_{2D \text{ unit cell}} = J \cdot d\zeta \quad (4-14)$$

$J$  is the line current density that is obtained by integration of scalar product of the current density  $\mathbf{j}$  with the normal vector  $\hat{\mathbf{n}}$  over the interface line.

Since the stack width is not infinitesimal, next step was to assume that actual design could be approximately modeled by letting the unit cell be homogeneously extended in the third dimension. This gave

$$I_{\text{extended unit cell}} = \int_{\zeta} J \cdot d\zeta = J \cdot \zeta \quad (4-15)$$

Ohmic contact losses were assumed to be negligible and are therefore not included. A circuit model for the extended unit cell, illustrated in Figure 4–4, was drawn and then extended into a stack circuit model. In order to reconstruct the original design,  $m$  layers with  $n$  extended unit cells connected in a series were assumed to be stacked upon each other and connected into a parallel circuit. This gave the voltage over the stack as  $n$  times larger than for the unit cell and the total current from the stack as

$$I_{stack} = m \cdot I_{extended\ unit\ cell} = m \cdot J \cdot \xi \quad (4-16)$$

Given that every unit cell has a defined size, the integers  $n$  and  $m$  together with the width  $\xi$  was identified as the parameters that sets the size of the stack. The volume becomes

$$V_{stack} = n \cdot x_{width} \cdot m \cdot y_{height} \cdot \xi \quad (4-17)$$

with a width of twelve millimeters and a height of  $150\ \mu\text{m}$ . Multiplication of the line current density with cell voltage then gave the power of each two dimensional cell as

$$P_{cell} = J \cdot V_{cell} \quad (4-18)$$

and analogous for the whole stack the expression for the power became

$$P_{stack} = n \cdot m \cdot J \cdot \xi \cdot V_{cell} \quad (4-19)$$

which can be identified as the power in each extended unit cell multiplied with the number of cells. Solving the model for several different values of the cell voltage, and

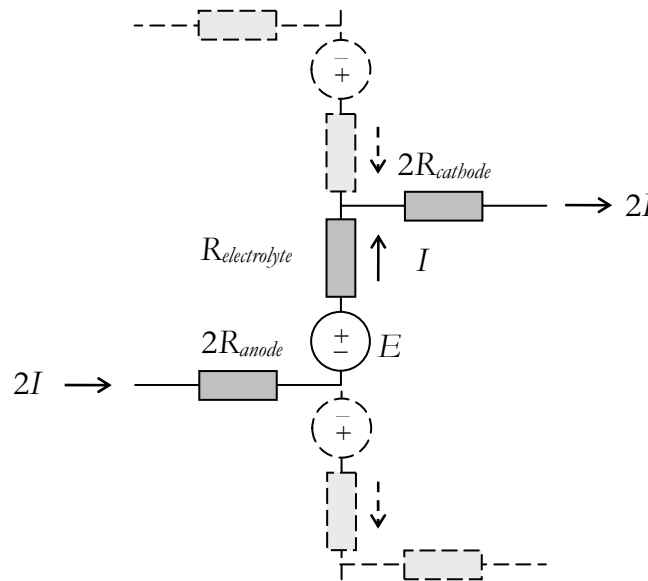


**Figure 4–4:** Unit cell circuit model. The current and the resistance are doubled over the electrodes since adjacent unit cells are reversed symmetric.

then plotting the cell power as a function of the line current density, determined the value for the maximum power and the corresponding line current density. The line current density was also plotted against the cell voltage in order to give the characteristics of the current-voltage relation.

#### 4.3.4 Ohmic Heat

The ohmic overpotential reveals that power is lost in the unit cell due to resistance. This also means that it appears as a heat source in the structure and that it had to be included in the heat transfer mode in the model. As mentioned in the theory chapter, this dissipated power can be calculated using Joule's law. Hence, expression (2–56) was combined with Ohm's law on point form given in section 2.5.3 into

$$Q = \mathbf{j} \cdot \frac{\mathbf{j}}{\sigma} = \frac{|\mathbf{j}|^2}{\sigma} \quad (4-20)$$

This was applied to all subdomains in the heat transfer mode with the proper values for sigma regarding the material.

#### 4.3.5 Approaches to Model the Consumption of Reactants

The current density  $\mathbf{j}$  on the electrolyte-electrode interfaces was also used to determine the amount of fuel and oxygen consumed in the fuel cell at each interface respectively. Regarding the change in pressure it could be a bit simplified since this gas was supposed to be ideal and that the net consumption of particles at anode-electrolyte interface was concluded to be zero since the amount of water and carbon dioxide produced are equal to the amount of reacting hydrogen and carbon monoxide respectively, in accordance with the theory 2.4.5. Due to this no pressure changes had to be considered at the anode-electrolyte interface.

However, this was not the case at the cathode-electrode interface where the reaction results in an outflow of oxygen molecules. This diffusion flux was added to the pressure mode using expression (2–60) on the horizontal cathode-electrolyte border. At the vertical interface no reaction outflow was assumed since it represents the outflow to the channel in that mode. Unfortunately this rather simple step in the building of the model caused problems for the solver algorithm, mainly due to difficulties in introducing couplings including derivatives. This problem was eventually solved using approximated values for the current density, but due to the limited time available and difficulties with getting Femlab to reset its initial values, this flux had to be set to zero in several calculations, and the pressure profile modeled as a one dimensional linear function. This was the case for the electrical characteristics presented in the following result chapter and it was therefore expected that they did not display any concentration overpotential. Since this was one of the main reasons for implementing diffusion flux in the Darcy law mode it has to be considered as a shortcoming in the modeling work.

Furthermore, the pressure profile was only one of two major aspects relating to the consumption of reactants that were to be modeled in order to describe the concentration polarization properly. It also included the change in the gas composition, which initially was intended to be intertwined with the mass transfer described by Darcy's law through the realization of the Dusty Gas Model, as mentioned before in the theory chapter and in

section 4.2.2. Disappointingly, no successful way for this implementation was found in Femlab and the consumption of the reactants had to be modeled separately with modes that also ran into the problem with derivative couplings.

The first approach to model the change of the gas composition was made using a Femlab mode based on Maxwell-Stefan diffusion, presented in section 2.2.4. Based on the theory 2.4.5, it was assumed that the proportions between hydrogen and carbon monoxide in the mixture remained constant. As it can be seen in Table 4–1 the relation is 2:1 for both hydrogen to carbon monoxide and for water to carbon dioxide. This simplification made it possible to model the anode gas with only three groups of gases instead all six species. The first group contained the consumed gases, hydrogen and carbon monoxide, the second the produced water and carbon dioxide and the third the remaining nitrogen and methane. In the cathode the two original species were modeled with an additional Maxwell-Stefan mode. Necessary gas parameters such as the binary diffusion coefficients were found in literature, as mentioned in 4.1.4.

However, the addition of the Maxwell-Stefan modes resulted in a prominent increase of the calculation time and the file size, which made the model more difficult to handle. And just as in the Darcy law mode, couplings involving the derivatives from the electrical modes had to be used at the electrode-electrolyte interfaces. Again this led to difficulties for the solution to converge and it was decided to replace these modes with two identical Femlab modes using a combination of diffusion and convection, based on a similar equation as the conduction and convection mode introduced in the Heating Mode, but formulated with the concentration as the free variable. In the anode three free variables were chosen and in the cathode mode two, in order to use the concept from the Maxwell-Stefan modes. After some revision the same diffusion coefficients were used in these modes as well. Regrettably this solution did not show any significant improvement compared to the Maxwell-Stefan approach.

Due to the limited time available for this project and the difficulties described above, it became necessary to make some simple approximations for the reactant consumption that could be included without adding too much complexity to the model. It was assumed that the amount of fuel and oxygen available decreased linearly from the inflow to the outflow in porous electrodes. The term used to describe the consumption of fuel in literature is *fuel utilization*, defined as the number moles consumed in the fuel cell divided by the number of moles available, and the typical value for an SOFC stack is 85 percent, with variations in the range of 70-90 percent [2, 12, 22, 23]. With these values as a basis, the fuel molar percentage in anode were set to decrease from 75 to 20 percent, giving a fuel utilization of 73 percent. This also meant that the proportion of water and carbon dioxide in the anode gas was set to increase from the initial 18 percent to 73 percent.

Naturally, a similar approximation had to be made for the oxygen consumption in the cathode. The values found in literature for this were more deviating than for the fuel utilization and typical figures were more difficult to identify. Nevertheless, it was decided to set the usage to ten percentage points giving it a variation from fifteen to five percent. The reason for setting the starting value lower than the original was to take into consideration the large amount of nitrogen that also is present in the cathode gas, and the diffusion gradient that arises for the oxygen directed towards the electrolyte.

### 4.3.6 Chemical Reaction Heat Generation

In order to describe the heat generated directly at the location of the chemical reactions, equation (2-73) was used. However, since it gave the heat generated by the overall reaction and not the actual process where the oxygen is ionized at the cathode and the rest of the reaction takes place at the anode, it was necessary to estimate the portion of it generated at each interface. No tabulated values were available anywhere in literature for the reaction entropy of the separate steps. Another problem was that the EMF was not available on both interfaces. As a simple approximation, the entropy at standard state was set to be equal on both sides, i.e. fifty percent of the overall reaction heat generated on both sides, and the deviating terms originating from the Nernst equation implemented where the partial pressures were available. This gave the following expression for the heat transferred to the fuel cell at the anode-electrolyte border

$$q = -T \left( \frac{\kappa_{H_2} \left( \frac{\Delta S_{H_2}^0}{2} + R \ln \frac{p_{H_2}}{p_{H_2O}} \right) + \kappa_{CO} \left( \frac{\Delta S_{CO}^0}{2} + R \ln \frac{p_{CO}}{p_{CO_2}} \right)}{\kappa_{H_2} + \kappa_{CO}} \right) \frac{\mathbf{j} \cdot \hat{\mathbf{n}}}{2F} \quad (4-21)$$

The corresponding expression at the cathode-electrolyte border became

$$q = T \left( \frac{\kappa_{H_2} \frac{\Delta S_{H_2}^0}{2} + \kappa_{CO} \frac{\Delta S_{CO}^0}{2}}{\kappa_{H_2} + \kappa_{CO}} + \frac{R}{2} \ln p_{O_2} \right) \frac{\mathbf{j} \cdot \hat{\mathbf{n}}}{2F} \quad (4-22)$$

without the negative sign due to the opposite directions of the current density and the normal vector at that interface.



## 5 Results

This section presents the results from the Femlab calculations on the Rutquist cell made with the developed model, first for the Heating Mode model and subsequently for the Active Mode model.

### 5.1 Heating Mode

This section presents the results from the calculations made for the warm-up of the Rutquist cell. As earlier described, this mode was initiated from room temperature and solved time-dependently.

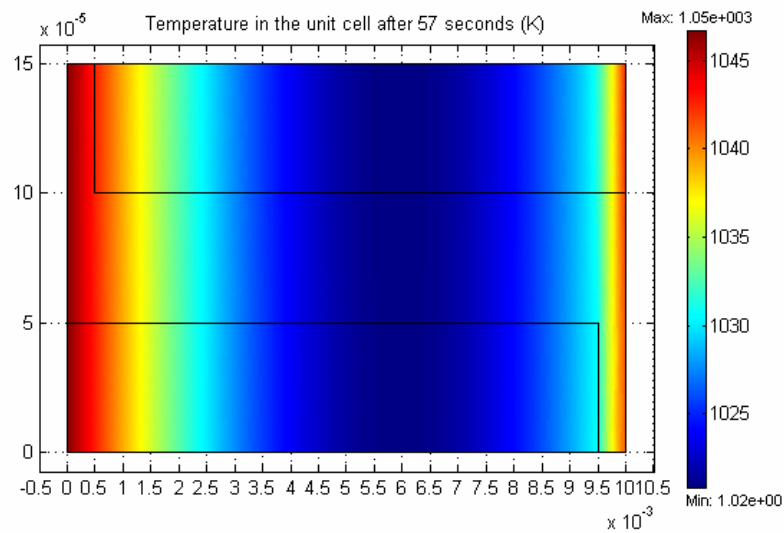


Figure 5-1: Temperature distribution after 57 seconds.

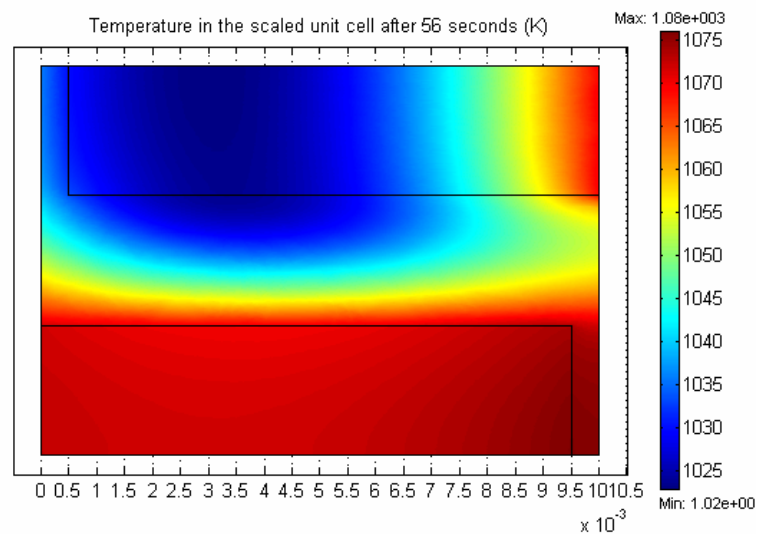
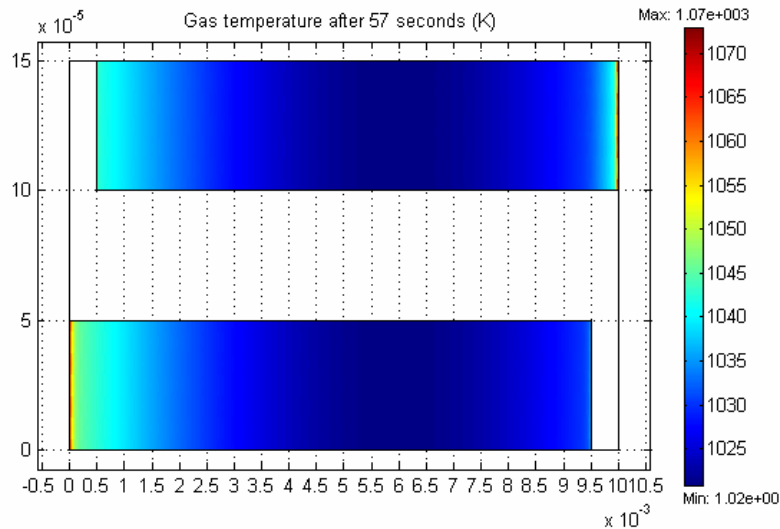


Figure 5-2: Temperature distribution in a scaled model after 56 seconds.



**Figure 5-3:** Gas temperature after 57 seconds.

### 5.1.1 Temperature profile

The main interest with the Heating mode model was to find the temperature distribution within the structure and to determine the time it takes until all parts of the structure has reached at least 1023 K, which is within fifty degrees from the working temperature. This heating time was calculated to 57 seconds.

Looking at Figure 5–1 it is interesting to see that the temperature is almost uniformly distributed in the vertical direction. Intuitively one might have expected a significant larger visible heat contribution from the warm gas in the electrodes.

In order to validate the model, the same calculation was made on a structure with different geometry presented in Figure 5–2. This scaled model is almost quadratic and it is clearly visible that there is a significant contribution from the gas in the electrodes. It is also possible to see the difference in temperature between the anode and the cathode due to the different thermal properties. It can however be noted that in the original model the length scale is more than sixty times smaller in the vertical direction than in the horizontal direction. The heat is rapidly conducted vertically and the small lateral differences in the temperature distribution seem to be leveled out.

The gas temperature and the temperature in the solid are closely connected and this is confirmed by the calculation of the gas temperature presented in Figure 5–3. Most of the heat from the gas is released close to the inflow of the electrode, and this effect is intensified by the contribution from the heat of the gas channels. The result is that the heat enters the unit cell from the sides and the spreads towards the middle, which is consistent with theory.

### 5.1.2 Pressure and velocity

The accuracy of the Conduction and Convection mode relies heavily on an adequate model of the gas diffusion through the electrodes. This is a problem that applies to the entire model, since the modes have strong couplings to each other, which cause a small error to propagate through the model and increase in size. To verify whether the Darcy

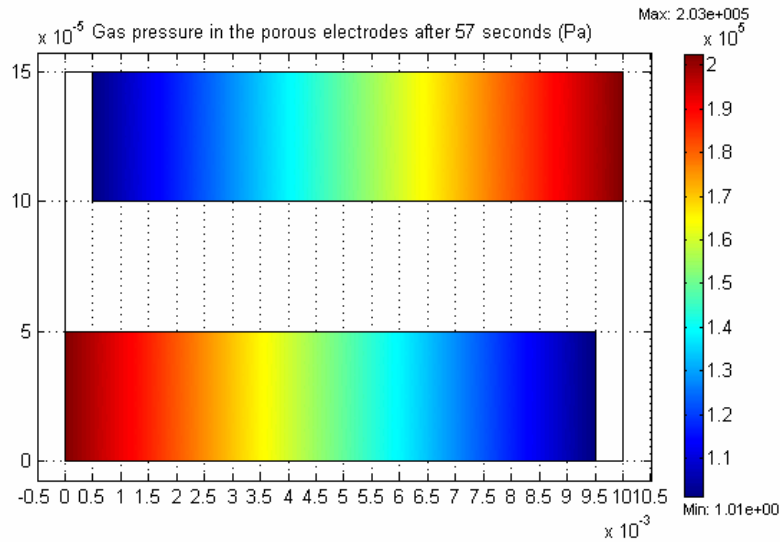


**Figure 5-4:** Gas pressure distribution in the porous electrodes after 57 seconds.

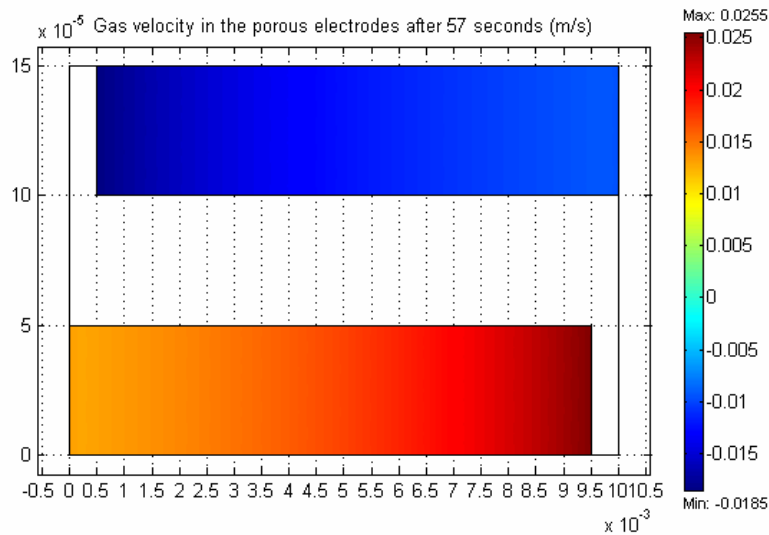


**Figure 5-5:** Gas velocity in the electrodes after 57 seconds.

law mode gave satisfactory results, the pressure distribution and the gas velocity were studied. Figure 5–4 shows the gas pressure in the electrodes after 57 seconds. The values range from twice the atmospheric pressure at the inlet to atmospheric pressure at the outlet. These values were set by the boundary conditions but the distribution in-between was calculated by the Darcy law mode.

Another way to determine whether the models hold or not, is to study conserved entities. Since gas is not consumed in the Heating Mode, the mass flux through the structure has to be constant according to the continuity equation. Now, looking at the gas velocity in Figure 5–5 and knowing that the temperature is almost constant over the electrode it is easy to establish that the model is working since the gas velocity at the outlet is twice that at the inlet. This follows from the pressure difference and that the concentration is proportional to the pressure since the temperature was approximated as

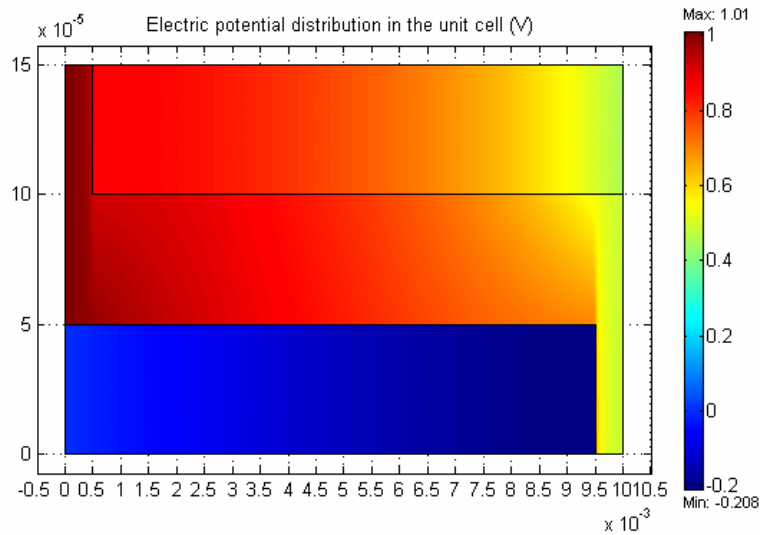


**Figure 5-6:** Voltage distribution at cell voltage 0.45 V and a uniform temperature of 1073 K.

constant in that step. To ensure a constant mass flux, the velocity has to be doubled at the outlet.

## 5.2 Active Mode

This section presents the results from the calculations made on the Rutquist cell during steady-state operation.

### 5.2.1 Electric Characteristics

Initially the electric characteristics of the unit cell were calculated with both the gas

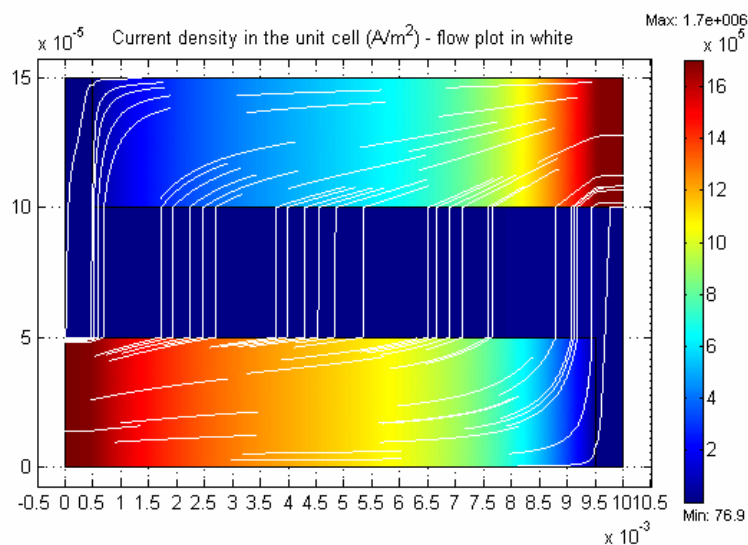


**Figure 5-7:** Current density at cell voltage 0.45 V and uniform temperature of 1073 K.

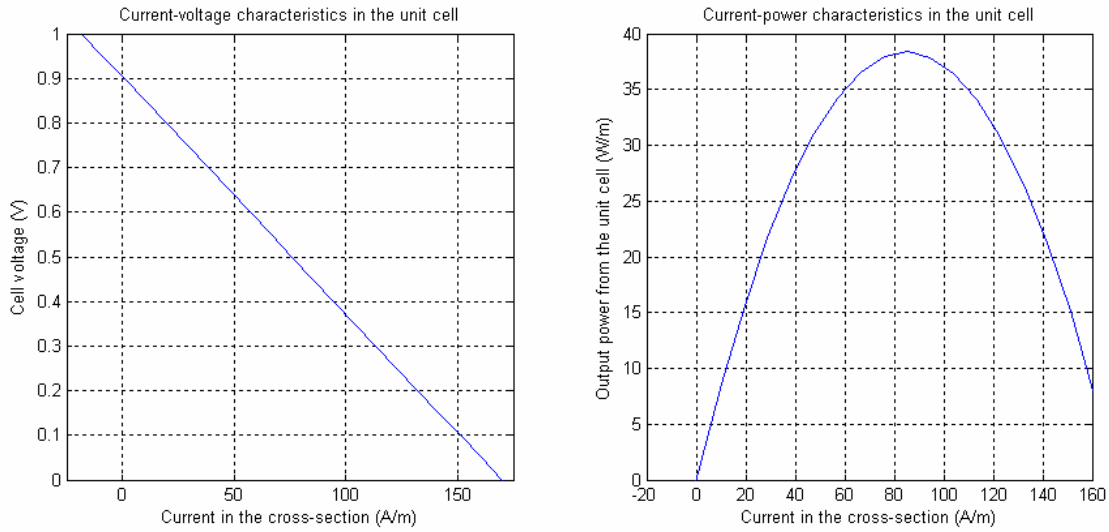


**Figure 5-8:** *Current-voltage relation (left) and current-power relation (right) for operation at uniform temperature of 1073 K.*

and the structure set to the assumed temperature of operation, 1073 K. The electric modes had been implemented as stated in section 4.3.2 and the same pressure profile as in the Heating Mode was used. The change in the gas composition due to consumption of gas reactants were modeled with a linear approximation based on the assumption of a certain fuel utilization in accordance with section 4.3.5. The attained potential distribution is presented in Figure 5–6 and the current density is shown in Figure 5–7 along with current flow lines.

Both Figure 5–6 and 5–7 are specified to the same cell voltage, 0.45 V. That value had been found to give the maximum power from the unit cell when the electrical modes previously were solved with the cell voltage varying between zero and one, in steps of 0.05 V. The line current density, defined in section 4.3.3, representing the two dimensional current was obtained by integration of the scalar product current density with normal vector on the border between cathode and the gas inflow channel, for each value of the cell voltage. The cell voltage was then plotted in Matlab as a function of the line current density. The result is displayed in Figure 5–8.

It can be seen that the current-voltage relation is linear which indicates that only ohmic polarization has been considered at this stage. Figure 5–8 also displays a plot of the current-power relation, calculated as presented in section 4.3.3 by multiplying each value for the line current density with the corresponding cell voltage. In this figure the maximum power was decided to be approximately 38 W/m at 0.45 V. In accordance with the theory in section 2.4.4 the current-power curve is parabolic.

From Figure 5–8 it was also concluded that the line current density corresponding to the maximal power was 85 A/m. These three values were then used to specify the necessary size for a stack to generate 10 kW. From section 4.3.3 it can be recalled that the width, height and depth of the stack was specified with the number of serial coupled cells  $n$ , the number of layers  $m$  and the depth  $z$ . Expression (4–19) was rewritten in order to decide a relationship between the three figures.

$$n \cdot m \cdot z = \frac{P_{stack}}{J \cdot V_{cell}} \Big|_{\text{maximum power}} \approx 260$$

Assuming that the stack was supposed to be quadratic, the following values were decided with the width of each unit cell, including the gas channels, set to twelve millimeters and the height set to 150  $\mu\text{m}$ . The result was

$$\begin{aligned} n &= 6 \\ m &= 540 \\ z &= 8 \text{ cm} \end{aligned}$$

and the dimensions became

$$V_{stack} \approx 7 \text{ cm} \times 8 \text{ cm} \times 8 \text{ cm}$$

The results from these calculations were then used when the complete Active Mode model was solved. As presented in sections 4.3.4 and 4.3.6 the current density had to be used in the heat transfer modes: for the ohmic heat in the Heat Transfer mode and for the heat generated by the chemical reactions in the Conduction and Convection mode. As previously mentioned that step caused problems, and approximations based on the current density profile given in Figure 5–7 were therefore used. Integration over the electrolyte subdomain gave the average current density as roughly 8100 A/m<sup>2</sup> in the electrolyte. Using the line current density at maximal power from above, the variation of the current density in the cathode was determined to vary from about zero at the left end to 1700 kA/m<sup>2</sup> at the right end. The variation in the anode was found similarly to shift from 1700 kA/m<sup>2</sup> at the left end to zero at the right end.

These figures were then implemented into the different heat modes of the Active Mode model instead of the derivative coupling. Solving the model at 0.45 V cell voltage now gave a modified value for the line current density at maximum power, namely 72 A/m and a new relationship between the figures  $n$ ,  $m$  and  $z$  was established.

$$n \cdot m \cdot z \approx 340$$

The new values became

$$\begin{aligned} n &= 7 \\ m &= 570 \\ z &= 8.5 \text{ cm} \end{aligned}$$

and the dimensions turned out to be

$$V_{stack} \approx 8.5 \text{ cm} \times 8.5 \text{ cm} \times 8.5 \text{ cm}$$

Even though these values differ somewhat from the results for the 10 kW stack when uniform temperature was assumed, the estimation of the cell volume is still well

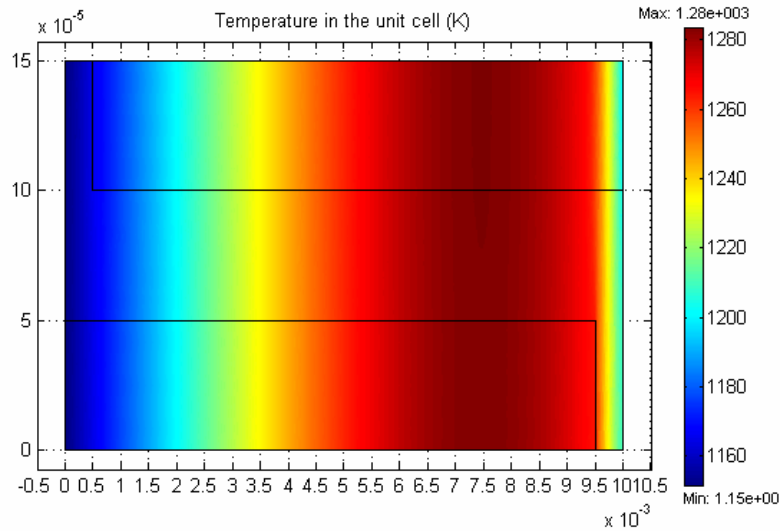


**Figure 5-9:** *The temperature distribution during operation.*

below  $1 \text{ dm}^3$ . This indicates that the Rutquist cell could be made very compact, with a power density above  $15 \text{ MW/m}^3$ .

### 5.2.2 Temperature profile

The original intention was to compute the temperature distribution in the structure during operation with all modes in function, including the Maxwell-Stefan mode and the Darcy law mode with correct boundary coefficients. However, as mentioned in many of the previous chapters and sections, no stable solution for this was attained. For this reason the final version of the complete Active Mode model used the linear approximation for the consumption of the reactants presented in 4.3.5 and, just as the first version, the same pressure profile as the Heating Mode. The current density was

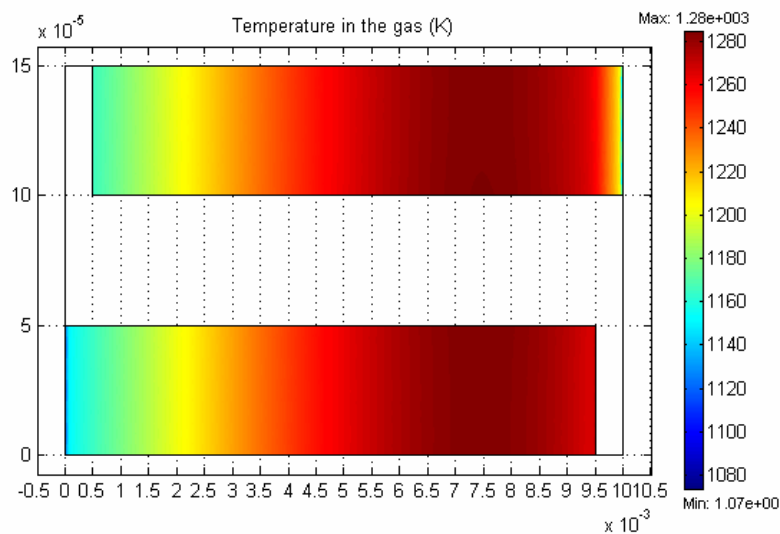


**Figure 5-10:** *The temperature distribution in the gases flowing through the electrodes.*

approximated with the results from the previous section for all for all other purposes than to couple the two different electric modes. The temperature distribution in the structure is presented in Figure 5–9 and the equivalent for the gases in the electrodes is presented in Figure 5–10.

The calculations showed that two the two main heat sources during operation, the ohmic heat and the heat generated by the chemical reactions, gave roughly the same contribution to the temperature. Unlike the result from the Heating Mode the gas flow through the electrodes now had taken the role of the cooling medium. It can be seen that the temperature variation in the cell goes from about 1160 K to 1280 K, a span of 120 K. Due to the couplings between the heat transfer modes, the profiles for the two different modes are very similar.



## 6 Discussion

This section of the report presents a reflection on the project done. It treats the framework set before the modeling work started along with the features in the model and the results it presented. It also includes a brief section about Femlab.

### 6.1 General overview

This section deals with the general scope and delimitations made before the modeling work was initiated and the consequences they brought about.

#### 6.1.1 The scope of the thesis

How realistic a model becomes obviously depends on the availability of accurate input and adequate theoretical models. No matter how good the models are, the result will still be misleading if the input parameters, such as material data, are incorrect. The opposite is also true, accurate input does not automatically generate realistic output if the models do not fully describe the processes.

Furthermore, in order to know which theories and models to use it is essential to have good knowledge of the physical phenomena and the environment in which they operate. For example, in the case of the electrodes and the gas diffusion, it was first after having established the nature of the material that a model, which correctly described the process at hand, could be found. The same holds for most physical processes; it is crucial to know the relevant parameters, and how they change with temperature and other external factors.

Bearing this in mind, and considering that this project stretch over such a large area of theory, it is understandable that the project time became one of the limiting factors for how well the model corresponds to reality. To this it can be added that the problems that arose during the implementation in Femlab also were time consuming.

#### 6.1.2 Delimitations and approximations

When modeling complex processes, limitations in computational power necessarily means that approximations have to be made. These simplifications introduce discrepancies from the wanted and more realistic results. It is therefore important to know how the approximations influence the outcome of the computations.

In the SOFC model the transformation from three dimensions to two actually reduced the time needed to heat the structure to working conditions. This is due to the choice of cross section and the way the gas channels are modeled. In reality is the distance between the inlet and the outlet probably 30-50 percent longer and the gas does not enter the electrodes over their whole width, but only from the circular gas channel openings. A 3-D model would also involve the three-dimensional spread of gas within the electrodes. All these factors would of course influence on the final result in a more complete model and probably give a prolonged heating time.

Due to the limited time at hand the model was divided into two modes, as mentioned earlier. This simplifying step was based on the assumption that these two separate parts would give desired information about the structure without losing too

much accuracy in relation to the model at large. Although this very likely is true, it naturally affects both the outcome of the model and the possibility to develop it further. If a more advanced model will be created, it shall preferably integrate the two parts into one.

One of the benefits with the separation of the model was that the chemical reactions could be excluded from the Heating Mode. They were assumed not to start before the all parts of the structure had reached at least 1023 K, but in reality they would have become important even before that due to successive initiation. This also implies that the current through the cell would grow gradually and since both these processes release energy to the cell, it would thus have helped warming the SOFC material. How much impact this would have on the time needed to reach full effect for the cell in comparison to the prolongation made by the 3-D to 2-D simplification, is difficult to tell, but could be a topic for further studies.

The choice to work with a repetitive element such as the unit cell, and determine properties for the entire stack from the results, implied that edge effects not could be considered. This introduced inaccuracy in the predictions of the model, however without challenging the main conclusions.

## ***6.2 Features in the model and its results***

This section discusses the choices made during in the modeling work, together with the results and predicted performance of the design made by Rutquist at Volvo Technology Corporation.

### **6.2.1 Tabulated data**

The governing principles for the material behavior in ceramics display big complexity, as for most materials. Generally the most important factor is the temperature. All material parameters are more or less dependent on the temperature. Despite this, the model work presented in this thesis has been done with constant values for all material data. As presented in sections 1.4.1 and 4.3.1 it was very difficult to find extensive data tables and this limited the possibilities to implement more complex relations. However, the data that was found is according to literature valid at the operating temperature and it can be assumed that these values are sufficiently correct when used in the temperature range of the Active Mode model. It could on the other hand be argued that the parameters are not correct in the Heating Mode model, especially the parameter bearing most uncertainty, the specific heat capacity. A more correct description of this parameter would have shortened the calculated time to heat the structure.

Most other tabulated values used, such as the gas parameters and the electromotive force at standard state for the reactions, are well supported and therefore not likely to be sources of errors.

### **6.2.2 Gas composition and diffusion**

One of the basic assumptions in the model is that fuel is fed from a reformer that converts diesel into usable substances for the fuel cell. The mixture originating from the reformer is both relevant and typical, but other compositions are also both possible and plausible. A thorough investigation of this is far beyond the scope of this thesis, but it

must be noted that variations in the composition would also alter the results. However, a change large enough to question the conclusions presented in the next section, is not very probable.

The gas diffusion ought to involve a more realistic model, preferably one where all the different gases diffuse individually according to the Dusty Gas Model described earlier. This will also give the fundament for a better model of the heat transfer within the structure. Moreover, separate gas diffusion would make it possible to look at the consumption of reactants and hence take a possible diffusion limitation of the chemical reactions and thereby also the concentration overpotential, into consideration.

A more successful implementation of the boundary conditions in the Darcy law mode and the overall Maxwell-Stefan modes would have given more realistic model than the linear profiles and approximations used for the pressure and the consumption of the reactants. Just as the Dusty Gas Model it would have taken the concentration overpotential into consideration in the model by supplying more correct values for the partial pressures into the Nernst expressions. A future model that includes these features will probably predict somewhat lower values for the maximum power and therefore also a larger stack in order to produce 10 kW. However, the prediction of the current model is definitely within the correct order of magnitude.

One plausible explanation to the difficulties in coupling the derivatives of the electric potential to the boundary conditions of the Darcy law mode is that the gas inlet pressure had been set to low. The solution would then have become too close to zero or even negative, which made the overall model impossible to solve. If this is true, it indicates that the chemical reactions would become diffusion limited very rapidly. Raising the gas inlet pressure would probably resolve the problem and cause an increased flow through the electrodes. It would in turn then increase the heat transfer from the gas to the structure and thus reduce the time needed to heat the structure in the Heating Mode as well as improve the cooling in Active Mode.

### 6.2.3 The Rutquist cell

The results presented, both for the Heating Mode and the Active Mode, illustrate the fact that the processes in the Rutquist cell in most cases can be seen as one-dimensional. This phenomenon is illustrated in both the heat and mass transfer modes as well as in the electric modes. Considering that the unit cell is almost sixty times wider than high, this is not very surprising. Several of the two-dimensional effects are leveled out due to the short vertical distance.

Moreover, the results of both model parts suggest that the assumed width of the electrodes ought to be increased. The temperature distribution difference between the scaled and original unit cell in the Heating Mode indicates that this would lower the warm up time through the cell due to increased heating from a larger gas flow together with the effect of an expanded volume with high thermal conductivity. This material parameter is almost twenty times larger in the anode compared to the electrolyte. In addition, in the Active Mode wider electrodes would, in the same way as an increased pressure difference, give better cooling of the structure and reduce the risk for concentration overpotential.

On the other hand, wider electrodes also would increase the volume necessary to accomplish a 10 kW stack with the Rutquist cell. But this cannot be regarded as a large setback considering that the presented model reveals that the design is very compact and even if it would become twice as big, it would still be very small in comparison to other

SOFC structures. Additionally, the difference in stack size between the preliminary Active Mode model, calculated with constant temperature in the electric modes, and the one with the correct temperature profile, also indicate that an increased cooling effect of wider electrodes would increase the performance, and make it possible to decrease the number of layers in the stack, as compensation.

Finally, it can be noted that the temperature distribution during operation corresponds well to the typical values for SOFC structures in general, according to literature.

### **6.3 Femlab**

The choice of modeling software plays a role in how a problem can be formulated. There is in general a trade off between the degree of freedom given in formulating the model specifications and the user friendliness. In Femlab's case much of the effort has been put on making the program intuitive and easy to work with, especially regarding smaller models. However, problems arise when many parameters are to be altered from their default values and when the models become larger. In addition, the system for handling and presenting mistakes and errors, that almost inevitably are encountered, is not sufficient. Too much of the project time was spent on debugging.

The coupling of the different modes to each other was a crucial factor in the modeling work. One hypothesis, which is both obvious and plausible, is that the number of couplings, and especially the derivative couplings, are critical for all the various Femlab solver types. The solutions were fine as long as only the electric modes used derivative couplings, but difficulties arose when the derivative of the electric potential were used in all other modes as well to describe the change in pressure and reactant fluxes along with the ohmic and chemical reaction heat.

A related aspect to the degree of coupling is the escalation of errors. When all equations and variables are intertwined, it is very important that all approximations and initial values are reasonable and correct. Otherwise the results become non-reliable or the problem impossible to solve.

It should also be noted that Femlab lack features for importing parameters between models and it demands for good computer capacity. If the latter is not available, even simple tasks such as saving or switching between modes, become very time demanding.

## 7 Conclusions

A model describing the Rutquist cell has been created that serves as an efficient analyzing tool. Several important features have been clarified and the model forms a good basis for further development. Nevertheless, due to the limited time available, simplifications and approximations have been made that lower the accuracy of the results. A more thorough description of the gas diffusion in the electrodes along with the concentration overpotential was desired. However, proposals on how to go further with the model have also been presented.

The Rutquist cell design allows a 10 kW stack to become very compact. According to the calculations made, using the acquired current-voltage characteristics of the unit cell along with a stack circuit model, the volume is less than one cubic decimeter. This is a very promising result and it clearly indicates that the design has a great potential in future APU applications.

The warm-up time for the unit cell calculated with the Heating Mode model was found to be less than one minute. The result is approximate and a more realistic description of the material parameters along with altered design parameters, such as increased gas inlet pressure and wider electrodes, would lower the time prediction. Moreover was the heating profile in the unit cell found one-dimensional, both during the warm-up process and the steady-state operation. This is due to the short vertical length of the unit cell that levels out any two-dimensional heat transfer. The ohmic heat and the chemical reaction were found to be the main heat sources during operation whereas the gas diffusing through the electrodes was established to bring about the main heating during warm-up. The temperatures displayed during operation are reasonable and comparable to other SOFC designs.

Femlab was found to have some drawbacks in this type of modeling work. The program will likely be much easier to manage when a proper and understandable system to handle and indicate implementation errors has been included. The difficulty in creating an attractive but at the same time powerful and flexible modeling program should however be recognized and the future prospects for Femlab are good.



## 8 Future Work

There are many ways to go further with the model at hand. The smallest and most simple step is probably to implement approximations for the current density into the Darcy law and Maxwell-Stefan mode in order to get an elementary consideration of the concentration overpotential. Besides that, there are many possibilities to work with the model in order to make it function without approximations and properly handle the derivative couplings. However, the best alternative in this matter would be to replace the existing diffusion modes with the Dusty Gas Model.

Another interesting opportunity is to examine the outcome of a larger pressure difference and wider electrodes. Regarding the cell design it can also be said that there is a need to examine it further to confirm the results presented in this thesis. In view of the fact that the model in so many cases displays one-dimensional features it would be a good idea to go further by building new 2-D models using other cross-sections. In a longer perspective a 3-D model is desirable, possibly taking the entire stack into account, including edge effects.

A combination of the warm-up and the operation model in which the chemical reaction starts successively and the material parameters change with temperature would also be an improvement of the model.

All of the suggestions above would make the current model more accurate in its predictions. The model need however also to be complemented with entirely new features in order to increase its usefulness. A proper stress analysis of the structure based on the temperature profiles would be of great interest.





## References

In this section all references used in the modeling work are listed. Three different types of sources have been employed: books, articles and Internet websites. The first part of the list gives the references cited in the report, in order of appearance. Following this, the general sources are stated in alphabetical order.

### *Cited Material*

- [1] Gellings P.J. and Bouwmeester H.J.M., editors. *The CRC Handbook of Solid State Electrochemistry*, Enschede, The Netherlands: CRC Press. (1997) ISBN 0-8493-8956-9.
- [2] McEvoy A. J., editor. Dobbs H., Krause T., Kumar R. and Krumpfelt M. Diesel-Fueled Solid Oxide Fuel Cell Auxiliary Power Units for Heavy Duty Vehicles. *Proceedings of the 4<sup>th</sup> European Solid Oxide Fuel Cell Forum*, Vol. 1, p. 85-95. (2000) ISBN 3-905592-04-5.
- [3] Badwal S.P.S., Bannister M.J. and Hannink R.H.J., editors. Minh N.Q., Solid Oxide Fuel Cells: Materials, Fabrication Processes and Development Trends. *Science and Technology of Zirconia V*, p. 652-663. Lancaster, PA, USA: Technomic Publishing Company, Inc. (1993) ISBN 1-56676-073-9.
- [4] Tritton D.J. *Physical Fluid Dynamics*, 2:nd ed., Bury St. Edmunds, Suffolk, UK: Oxford University Press. (1995) ISBN 0-19-854493-6.
- [5] Welty J.R., Wicks C.E. and Wilson R.E. *Fundamentals of Momentum, Heat, and Mass Transfer*, 3:rd ed., New York, NY, USA: John Wiley & Sons Ltd. (1988) ISBN 0-471-87497-3.
- [6] Krishna R. and Wesselingh J.A. The Maxwell-Stefan Approach to Mass Transfer. *Chemical Engineering Science*, Vol. 52, No. 6, p. 861-911. (1997) ISSN 0009-2509.
- [7] Shelby J.E. *Handbook of Gas Diffusion in Solids and Melts*, Materials Park, OH, USA: ASM International. (1996) ISBN 0-87170-566-4.
- [8] *FEMLAB Chemical Engineering Module*, Version 2.3, Stockholm, Sweden: Comsol AB. (2002)
- [9] Todd B. and Young J.B. Thermodynamic and Transport Properties of Gases for Use in Solid Oxide Fuel Cell Modelling. *Journal of Power Sources*, Vol. 110, p. 186-200. (2002) ISSN 0378-7753.
- [10] Koh J.-H., Seo H.-K., Yoo Y.-S. and Lim H.C. Consideration of Numerical Simulation Parameters and Heat Transfer Models for a Molten Carbonate Fuel Cell Stack. *Chemical Engineering Journal*, Vol. 87, p. 367-379. (2002) ISSN 1358-8947.

- [11] McEvoy A. J., editor. Selimovic A., Yuan J. Rokni M., Sundén B., Pålson J., Torisson T. and Sjunnesson L. Analysis and Effects of Heat Transfer and Friction Factor on SOFC Performance Characteristics. *Proceedings of the 4<sup>th</sup> European Solid Oxide Fuel Cell Forum*, Vol. 1, p. 403-412. (2000) ISBN 3-905592-04-5.
- [12] Hirschenhofer J.H., Stauffer H.K., Engleman R.R. and Klett M.G. *Fuel Cell Handbook*, USA: Parsons Corporation, U.S. Department of Energy. (1998) DOE/FETC-99/1076.
- [13] Minh N.Q. and Takahashi T. *Science and Technology of Ceramic Fuel Cells*, Amsterdam, The Netherlands: Elsevier Science B.V. (1995) ISBN 0444-89568X.
- [14] Atkins P.W. *Physical Chemistry*, 3:rd ed., Chichester, Sussex, UK: Oxford University Press. (1986) ISBN 0-19-855186-X.
- [15] Chemistry Learning Center – *Equilibrium*  
URL: <http://learn.chem.vt.edu/tutorials/equilibrium/index.html>  
(2002-11-05)
- [16] NASA Glenn Research Center – Chemical Equilibrium with Applications  
URL: <http://www.grc.nasa.gov/WWW/CEAWeb/>  
(2002-11-25)
- [17] Hibbert D.B. *Introduction to Electrochemistry*, Chatham, Kent, UK: MacMillan Press Ltd. (1993) ISBN 0-333-56303-4.
- [18] Hamann C.H., Hamnett A. and Vielstich W. *Electrochemistry*, Mörlenbach, Germany: Wiley-VCH Verlag GmbH. ISBN 3-527-29095-8. (1998)
- [19] Cheng D.K. *Fundamentals of Engineering Electromagnetics*, Reading, MA, USA: Addison-Wesley Publishing Company, Inc. (1993) ISBN 0-201-56611-7.
- [20] Amphlett J.C., Mann R.F., Peppley B.A., Roberge P.R., Rodrigues A. and Salvador J.P. Simulation of a 250 kW Diesel Fuel Processor/PEM Fuel Cell System. *Journal of Power Sources*, Vol. 71, p. 179-184. (1998) ISSN 0378-7753.
- [21] Docter A. and Lamm A. Gasoline Fuel Cell Systems. *Journal of Power Sources*, Vol. 84, p. 194-200. (1999) ISSN 0378-7753.
- [22] Campanari S. Thermodynamic Model and Parametric Analysis of a Tubular SOFC Module. *Journal of Power Sources*, Vol. 92, p. 26-34. (2001) ISSN 0378-7753.
- [23] McEvoy A. J., editor. Campanari S. Simulation and Thermodynamic Analysis of a Tubular SOFC Module. *Proceedings of the 4<sup>th</sup> European Solid Oxide Fuel Cell Forum*, Vol. 1, p. 393-402. (2000) ISBN 3-905592-04-5.

- [24] Pietsch E.H.E., Meyer R.J. and Kotowski A., editors. *Gmelins Handbuch der Anorganischen Chemie Cells – Zirkonium*, No. 42, 8:th ed., Lübeck, Germany:Verlag Chemie, GmbH. (1958)
- [25] Nordling C. and Österman J. *Physics Handbook for Science and Engineering*, 2:nd ed., Lund, Sweden: Studentlitteratur. (1996) ISBN 91-44-16575-7.
- [26] Shchurov A.F. and Perevoshchikov V.A. Mechanical Properties of Ytria-stabilized Zirconia Crystals. *Inorganic materials*, Vol. 33, p. 920-923. (1997) ISSN 0020-1685.

## General Sources

Aguiar P., Chadwick D. and Kershenbaum L. Modelling of an Indirect Internal Reforming Solid Oxide Fuel Cell. *Chemical Engineering Science*, Vol. 57, p. 1665-1677. (2002) ISSN 0009-2509.

Badwal S.P.S., Bannister M.J. and Hannink R.H.J., editors. Eguchi K., Setoguchi T., Tamura S. and Arai. H., Solid Oxide Fuel Cell with a Thin Stabilized Zirconia Film Supported on Electrode Substrate. *Science and Technology of Zirconia V*, p. 694-703. Lancaster, PA, USA: Technomic Publishing Company, Inc. (1993) ISBN 1-56676-073-9.

Badwal S.P.S., Jiang S.P., Love J., Nowotny J., Rekas M., Vance E.R. A Manometric Method for the Determination of Chemical Diffusion in Perovskite-type Cathode Materials for the Solid Oxide Fuel Cell. *Ceramics International*, Vol. 27, p. 431-441. (2001) ISSN 0272-8842.

Brander O. *Vektoranalys – Modellering av fysikaliska problem i tre dimensioner*, Lund, Sweden: Studentlitteratur. (1995) ISBN 91-44-48631-6.

Capek P. and Seidel-Morgenstern A. Multicomponent Mass Transport in Porous Solids and Estimation of Transport Parameters. *Applied Catalysis A: General*, Vol. 227, p. 227-237. (2001) ISSN 0926-860X.

Cyberspace Chemistry (CaCt) – *Nernst Equation*  
 URL: <http://www.science.uwaterloo.ca/~cchieh/cact/c123/nernsteq.html>  
 (2002-10-31)

Divisek J., de Haart L.G.J., Holtappels P., Lennartz T., Malléner W., Stimming U. and Wippermann K. The Kinetics of Electrochemical Reactions on High Temperature Fuel Cell Electrodes. *Journal of Power Sources*, Vol. 49, p. 257-270. (1994) ISSN 0378-7753.

*FEMLAB Model Library*, Version 1.1, Stockholm, Sweden: Comsol AB. (1999)

*FEMLAB Reference Manual*, Version 2.2, Stockholm, Sweden: Comsol AB. (2001)

*FEMLAB User's Guide and Introduction*, Version 2.0, Stockholm, Sweden: Comsol AB. (2000)

Heuer A.H. and Hobbs L.W., editors. Subbaro E.C. Zirconia – an Overview. *Advances in Ceramics – Science and Technology of Zirconia*, Vol. 3. Columbus, OH, USA: The American Ceramic Society, Inc. (1981) ISBN 0-916094-42-1.

Ivers-Tiffée E., Weber A. and Herbristrit D. Materials and Technologies for SOFC - components. *Journal of European Ceramic Society*, Vol. 21, p. 1805-1811. (2001) ISSN 0955-2219.

Lehnert W., Meusinger J. and Thom F. Modelling of Gas Transport Phenomena in SOFC Anodes. *Journal of Power Sources*, Vol. 87, p. 57-63. (2000) ISSN 0378-7753.

Mandl F. *Statistical Physics*, 2:nd ed., Plymouth, Devon, UK: John Wiley & Sons Ltd. (1988) ISBN 0-471-91532-7.

McEvoy A. J., editor. Ackman T., de Haart L.G.J. Lehnert W. and Thom F. Modelling of Mass and Heat Transport in Thin-Electrolyte Layer SOFCs. *Proceedings of the 4<sup>th</sup> European Solid Oxide Fuel Cell Forum*, Vol. 1, p. 431-438. (2000) ISBN 3-905592-04-5.

McEvoy A. J., editor. Stolten D., Froning D. and de Haart L.G.J. Modelling of Planar Anode-Supported Thin-Layer Stacks. *Proceedings of the 4<sup>th</sup> European Solid Oxide Fuel Cell Forum*, Vol. 1, p. 347-354. (2000) ISBN 3-905592-04-5.

Pietsch E.H.E., Meyer R.J. and Kotowski A., editors. *Gmelins Handbuch der Anorganischen Chemie Cells – Magnetische Werkstoffe*, No. 58, 8:th ed., Lübeck, Germany:Verlag Chemie, GmbH. (1959)

Ralph J.M., Schoeler A.C. and Krumfelt M. Materials for Lower Temperature Solid Oxide Fuel Cells. *Journal of Materials Science*, Vol. 36, p. 1161-1172. (2001) ISSN 0022-2461.

Råde L. and Westergren B. *Mathematics Handbook for Science and Engineering*, 3:rd ed., Lund, Sweden: Studentlitteratur. (1995) ISBN 91-44-25053-3.

# Glossary

**Activation Polarization** – Contribution to the polarization due to an energy barrier that the species must overcome in order for chemical reactions to take place.

**Active Mode** – SOFC model for the Rutquist cell during steady-state operation.

**Anode** – The part of the fuel cell from which positive charges enter, or negative charges leave the electrolyte. Incoming gas is oxidized. Also, see Electrodes.

**APU** – Auxiliary Power Unit. A device that supplies complementary power in vehicles for other purposes than transport.

**Autothermal Reformer** – A device in which fossil fuel is reformed using a mixture of steam and oxygen. Different reactions supply and expend heat simultaneously. See Reformer.

**Binary Diffusion** – Diffusion of two interacting species.

**Boundary Mode** – A Femlab application interface in which the parameters of the subdomain boundaries can be adjusted. Also, see Subdomain and Femlab.

**Bulk Diffusion** – Predominant diffusion mechanism for a dense gas mixture in material with relatively large pores.

**Cathode** – The part of the fuel cell from which negative charges enter, or positive charges leave the electrolyte. Incoming gas is reduced. Also, see Electrodes.

**Cermet** – Ceramic metal mixture.

**Channel Flow** – Viscous incompressible flow between two parallel walls in 2-D.

**Concentration Polarization** – Contribution to the polarization due to lowered concentration of reactants at the reaction site.

**Diffusion Constant** – Synonym to diffusivity. See Diffusivity.

**Diffusion Limited Reactions** – Chemical reactions limited by the mass transport rate.

**Diffusivity** – The rate of movement of an individual specimen in comparison to the medium in which it is transferred, given in  $m^2/s$ .

**Dusty Gas Model** – A diffusion model for multicomponent diffusion through a porous medium that can be combined with the consumption of chemical reactants.

**Electrode** – Common word for the anode and cathode in an electro-chemical cell. Both display electronic conduction.

**Electrolyte** – The ion-conducting compartment between the anode and the cathode in an electrochemical cell.

**Electromotive Force** – The potential difference over the electrolyte that arises due to electrochemical reactions. The open circuit voltage of an electrochemical cell.

**Electronic Conduction** – Electric conduction that occurs through transport of electrons or holes.

**EMF** – See Electromotive Force.

**Entropy** – The degree of energy degradation in a system.

**Femlab** – Computational software using finite element methods.

**Femlab Modes** – Modules in Femlab that govern specific physical or chemical processes.

**Fick Diffusion** – Diffusion governed by Fick's law. In a porous media also named bulk diffusion. See Bulk Diffusion.

**Film** – A thin laminar layer adjacent to the wall that occurs in pipe and channel flow regardless of the main flow type.

**Film Coefficient** – The convection coefficient calculated in a film, using the flow properties. Also, see Film.

**Fluid** – A substance that deforms continuously when exposed to shear stress.

**Forced Convection** – Energy exchange between a surface and an adjacent fluid when the fluid is forced to flow past the surface.

**Free Convection** – Energy exchange between a surface and an adjacent fluid when temperature differences cause the fluid circulation.

**Fuel Utilization** – Molar fraction of the consumed fuel at the inlet to the remaining fuel at the outlet.

**Fully Developed Flow** – The velocity profile of the flow does not vary along the line of the flow.

**Gibb's Free Energy** – The change in free enthalpy for a reaction, i.e. the part that has not contributed to entropy. The reaction is spontaneous if this entity is negative.

**Heat Expansion Coefficient** – Coefficient describing the relation between a change in temperature and the expansion of a material

**Heating Mode** – SOFC model that describes the Rutquist cell when being heated from 293 K to 1023 K, the assumed temperature for the initiation of chemical reactions in the cell.

**Ionic Conduction** – Electric conduction that occurs through transport of ions.

**Knudsen Diffusion** – Predominant diffusion mechanism when the mean free path of the diffusing molecules is much larger than the diameter of the pores.

**Laminar Flow** – Well ordered flow in which the movement occurs in layers positioned in the direction of the flow. Arise for low Reynolds numbers.

**Matlab** – Computational matrix based software.

**Mesh Mode** – A Femlab application interface in which the mesh parameters can be adjusted. Also, see Subdomain and Femlab.

**Molecular Diffusion** – Mass transport of molecules. See Bulk, Knudsen and Surface Diffusion for the different types possible in a porous media.

**Multicomponent Diffusion** – Diffusion of several interacting species.

**Multiphysics** – A Femlab modeling system based on the combination of modes describing various physical phenomena. Also, see Femlab and Femlab Modes.

**Nernst Potential** – Alternative name for EMF. See Electromotive Force.

**Nusselt Number** – Dimensionless parameter describing the ratio of conductive thermal resistance to convective thermal resistance  $a$  in a fluid.

**Ohmic Polarization** – Contribution to the polarization due to the resistance to electric flow in the structure.

**Overpotential** - The difference between the EMF and the actual cell voltage. It is equal to the sum of the different polarizations.

**Permeability** – Measure of the capacity to transmit fluids in a porous medium, given in  $m^2$ .

**Physical Diffusion** – The diffusing species do not interact chemically unless they are present simultaneously at a favorable reaction site.

**Pipe Flow** – Viscous incompressible flow through a tube of uniform circular cross-section.

**Polarization** – See Overpotential.

**Porosity** – The fractional amount of void space in a material.

**Reaction Enthalpy** - The change in energy carried by the reactants before and after a chemical reaction.

**Reaction Limited Reactions** – Chemical reactions limited by the reaction rate.

**Reformer** – A device for the conversion of liquid or gaseous fossil fuel to a desired gas mixture.

**Reversible Reaction** – A reaction that does not generate entropy.

**Reynolds Number** – Dimensionless parameter describing different types flow. High Reynolds numbers indicate turbulent flow, whereas low indicate laminar flow.

**SOFC** – Solid Oxide Fuel Cell. A type of high temperature ceramic electrochemical cell.

**Solvent** – Substance that dissolves another substance.

**Stack** – Assembly of several fuel cell elements.

**Standard State** – The pure form of a substance at unit pressure for a given temperature.

**Standard Voltage** – The EMF at standard state.

**Subdomain** – Geometric section in a Femlab model. To each subdomain different material data and modes can be applied. Also, see Femlab Modes and Subdomain Mode.

**Subdomain Mode** – A Femlab application interface in which the subdomain parameters can be adjusted. Also, see Subdomain and Femlab.

**Surface Diffusion** – Diffusion where adsorbed molecules are forced to move due to two-dimensional concentration gradients.

**Triple Phase Boundary** - The triple phase boundary refers to the surface where the electrolyte meets the porous electrode.

**Turbulent Flow** – Chaotic flow without any regular paths that occurs for high Reynolds numbers.

**Tortuosity** – Property linking actual path length to nominal length of a porous media.

**Yttria** – Yttrium oxide,  $Y_2O_3$ . A type of ceramic material. See Yttrium.

**Yttrium** – Metallic element number 39, Y.

**Zirconia** – Zirconium oxide,  $ZrO_2$ . A type of ceramic material. See Zirconium.

**Zirconium** – Metallic element number 40, Zr.

## Appendix A: Material Parameters

This table presents the material parameters found during the literature study. All values except  $C_p$  are valid at 1073 K. The values for  $C_p$  are valid at 25 °C.

Material	YSZ (8 mol%)	Ni/YSZ cermet	LaMnO <sub>3</sub>
----------	--------------	---------------	--------------------

Component	Electrolyte	Anode	Cathode
-----------	-------------	-------	---------

$\alpha$ - thermal expansion coefficient [m/(m K)]	10.8e-6 [13 (p.88)]	12.5e-6 [13 (p. 149)]	11.2e-6 [13 (p. 122)]
$C_p$ (T) - specific heat capacity [J/(kg K)]	563 [24 (p. 232)]	527 [24, 25 (T1.1)]*	480 [25]**
$\rho$ - density [kg/m <sup>3</sup> ]	5900 [13 (p. 75)]	5900 [13 (p. 75)]	6570 [13 (p. 122)]
$E$ - Young's modulus [GPa]	210 [26]		
$k$ - thermal conduction [W/(m K)]	2 [13 (p. 75)]	28 [13, 25 (T1.1)]*	4 [13 (p. 122)]
$\sigma$ - electrical conductivity [1/( $\Omega$ m)]	10 [13 (p. 80)]	5e4 [13 (p. 149)]	1.6e4 [1 (p. 414)]

The number inside the angle brackets gives the number of the reference given in the reference list. The clarification in the parenthesis gives the page number or table in the reference.

\* Linear interpolation with 30% Ni and 70% YSZ: 0.3×value for Ni + 0.7×value for YSZ

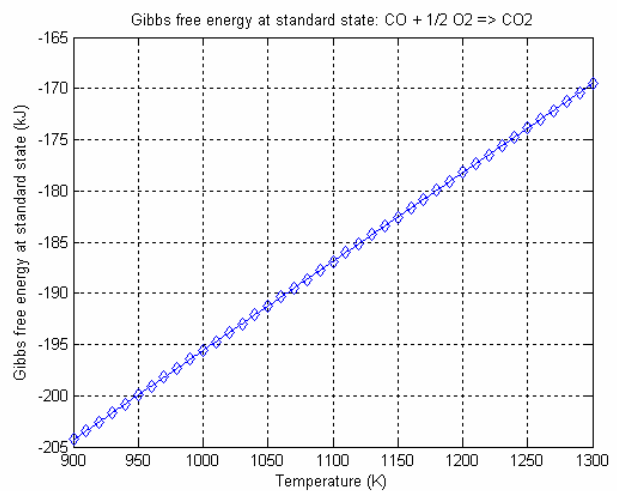
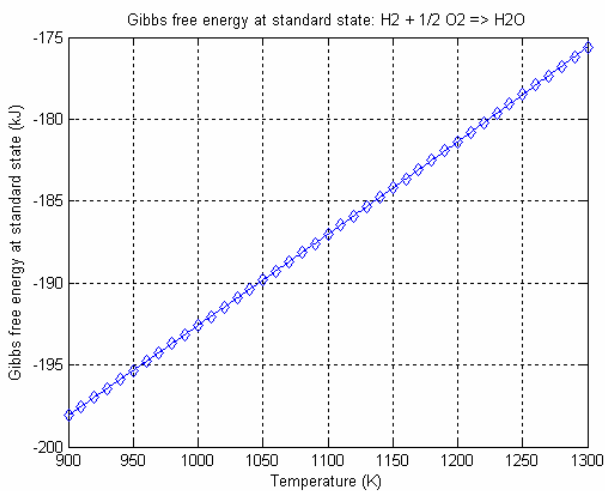
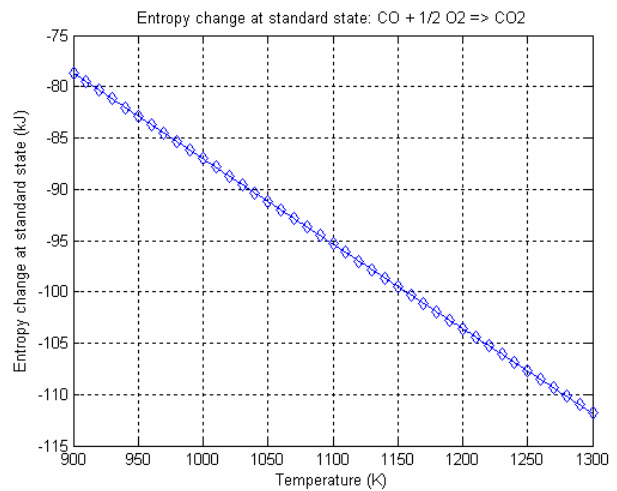
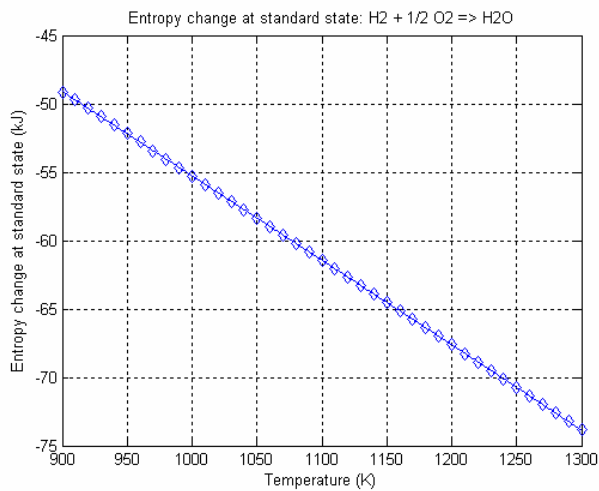
\*\* This value is a guess based on the value for manganese (Mn), but it corresponds well to several other oxides.





## Appendix B: Standard State EMF Polynomial Curve Fits

The graphs presented below represents the second order polynomial curve fits that were made in Matlab for the electromotive force at standard state based on the CEA program [16], as presented in section 4.3.2. Values are given in kJ for the temperature span 900-1300 K. The two graphs on top shows the entropy change for the hydrogen to water reaction (on the left) and the carbon monoxide to carbon dioxide reaction (on the right). Below is the Gibb's free energy change found for the hydrogen to water reaction (on the left) and the carbon monoxide to carbon dioxide reaction (on the right). The lines represent the values given by the CEA program and the diamonds the curve fits.





# Appendix C: Log Function Polynomial Curve Fit

The graph presented below represents the third order polynomial curve fit that was made in Matlab for the logarithmic function in order to simplify the Femlab calculations as presented in section 4.3.2. The line represents the actual profile of the logarithmic function and the diamonds the curve fit.

